Theoretical aspects of dipolar interactions and their appearance in first-order reversal curves of thermally activated single-domain particles

R. Egli[1]

Received 14 June 2006; revised 13 October 2006; accepted 30 October 2006; published 12 December 2006.

[1] Recently, the study of interacting particles was driven by the modeling effort undertaken to interpret first-order reversal curve (FORC) diagrams of natural rocks and sediments. Understanding the effect of magnetostatic interactions is of primary importance in rock magnetism and paleomagnetism, and FORCs can provide useful information for this purpose. However, fully quantitative theories of FORC measurements have not been formulated yet. The goal of this paper is to fill this gap for the case of interacting single-domain (SD) particles. First, a general analytical expression is obtained for the local interaction field produced by a random set of magnetic dipoles. This expression is then used to formulate a general theory that explains the effect of the local interaction field on FORCs. Exact solutions are obtained for the case of weakly interacting single-domain particles, whereby the effect of thermal activations is considered as well. These solutions show that a rigorous analysis of the FORC function and its relationship with the distributions of coercivities and interaction fields is possible.

Citation: Egli, R. (2006), Theoretical aspects of dipolar interactions and their appearance in first-order reversal curves of thermally activated single-domain particles, *J. Geophys. Res.*, *111*, B12S17, doi:10.1029/2006JB004567.

1. Introduction

[2] Many properties of magnetic grain assemblages are influenced by magnetostatic interactions, defined as the sum of all dipole-dipole interactions between the grains. One possible approach to modeling systems of interacting particles is based on the introduction of the so-called local interaction field (IF) $\mathbf{H}_i$, defined as the field produced in the volume occupied by a given grain by all other grains. Given the random geometric arrangement of magnetic particles in many natural and synthetic materials, the local IF is conveniently regarded as a statistical variate with a probability density function (PDF) $W(\mathbf{H}_i)$ that depends on the magnetization state of the sample. This description of magnetostatic interactions is the fundament of models aiming to explain the magnetic properties of random fine particle and spin systems whose coupling strength is not sufficient to produce a collective behavior (a state called ''quenched randomness'' by *Sornette* [2004]). The magnetic properties of these systems are effectively modeled by accounting for the effect of the IF distribution (IFD) on the intrinsic properties of the particles. A well-known example of this approach is the Preisach model, which describes hysteresis loops in terms of elemental rectangular loops [*Preisach*, 1935; *Néel*, 1954].

[3] Magnetostatic interactions have strong effects on weak-field magnetizations, such as the anhysteretic and the thermal remanent magnetization (ARM and TRM), even in diluted assemblages of grains, as established both experimentally [*Sugiura*, 1979] and theoretically [*Shcherbakov and Sycheva*, 1996; *Egli*, 2006]. Magnetic properties related to relaxation effects, such as viscous magnetizations (VRMs), and the low-field susceptibility of superparamagnetic particles, are also affected by interactions [e.g., *Dormann et al.*, 1997]. Despite the evident implications in paleomagnetism, rock magnetism and environmental magnetism, quantitative modeling of magnetostatic interactions in rocks and sediments is severely limited by the intrinsic heterogeneity of these materials, and the lack of knowledge about the spatial distribution of the magnetic carriers within the volume of the sample.

[4] New attention to the characterization of magnetostatic interactions was brought in by the introduction of first-order reversal curve (FORC) diagrams [*Mayergoyz*, 1986]. An intense modeling effort is now undertaken to understand FORC distributions of fine particle systems [e.g., *Pike et al.*, 1999, 2001; *Muxworthy and Williams*, 2005; *Newell*, 2005], and identify them in natural materials [*Roberts et al.*, 2000]. The use of FORC diagrams is particularly appealing, since it allows, under certain circumstances, to reconstruct the intrinsic properties of fine particle systems.

[5] Realistic models of hysteretic and anhysteretic processes in magnetic particle systems are extremely complex, because of the need of taking into account various physical processes, such as the reversing mechanism and its dependence on grain size, shape and orientation, the effect of thermal activations, and, finally, magnetostatic interactions. Since each of the abovementioned mechanisms is complex, all present models deal with some simplifications, such as

[1]Institute for Rock Magnetism, University of Minnesota, Minneapolis, Minnesota, USA.

0148-0227/06/2006JB004567$09.00

the assumption of aligned particles, or a coherent rotation reversal mechanism. Numerical calculations of the IF in large systems of n particles are computationally expensive, the number of required operations being proportional to n^2. An analytical expression for the local IF can introduce significant simplifications in models of interacting particles, and is unavoidable in the cases where the numerical approach is impractical, such as in modeling the ARM of interacting fine particles [*Egli*, 2006]. A rigorous approach to the calculation of the IF was introduced by *Anderson* [1950], with later contributions by *Shcherbakov and Shcherbakova* [1975] and *Berkov* [1996]. A semianalytical approximation was obtained for the IFD in the two limit cases of random assemblages of very diluted and very concentrated particles, respectively. However, intermediate cases of magnetic grains that occupy 1.5–20% of the sample's volume are still unsolved.

[6] The first purpose of this paper is to obtain an expression for $W(\mathbf{H}_i)$ that is generally valid at all concentrations. This expression applies to assemblages of particles that (1) can be modeled as magnetic dipoles, and (2) are randomly distributed within a given volume. Since $W(\mathbf{H}_i)$ depends on the magnetization state of the particles, three common configurations of the magnetic moments will be considered: (1) the case of randomly oriented dipoles, (2) the case of aligned dipoles, and (3) the case of random dipoles confined into a plane perpendicular to the direction of measurement. I will show that the three cases can be used to estimate the local interaction field distribution when an external field is applied.

[7] I will then use the analytical estimate of the IFD to model the effect of dipole interactions on the shape of FORC functions. Solutions of this model for weakly interacting single-domain (SD) particles with and without thermal activations provide an insight on the relationship between the FORC function and intrinsic properties of the particles, such as the distribution of coercivities and the packing fraction.

2. IF of Randomly Oriented Dipoles

[8] Consider a sphere of radius R that contains n randomly distributed, nonoverlapping identical grains of diameter ρ, each carrying a magnetic dipole moment $\mathbf{m}_i$. The grains are made of a material with saturation magnetization μ_s, thus having a magnetic moment $m = \pi\mu_s\rho^3/6$. The directions of the magnetic moments are random. Following the approach of *Shcherbakov and Shcherbakova* [1975] and *Berkov* [1996] it is possible to consider a system of n dipoles as the superposition of n systems made of a single dipole $\mathbf{m}$ at a random position $\mathbf{r}$, located in a sphere of radius R. However, as noted by *Berkov* [1996], the finite dimension of the grains implies a correlation of their positions, imposed by the nonoverlapping condition $|\mathbf{r}_i - \mathbf{r}_j| \geq \rho$ for every couple (i,j) of dipoles. I will show that the spatial correlation can be accounted by a simple modification of $W(\mathbf{H}_i)$ calculated for uncorrelated particles. Therefore the first step consists in the calculation of the IFD produced by a single dipole with $\rho \leq |\mathbf{r}| \leq R$. The central limit theorem is then used to calculate the IFD produced by n dipoles.

2.1. Field Produced by a Single Random Dipole

[9] I assume without loss of generality that the center of a spherical volume is occupied by one grain. The field produced by another grain at a random position in the sphere is to be calculated. I therefore introduce a randomly oriented point dipole with moment $\mathbf{m}$, whose position $\mathbf{r}$ is randomly chosen between two concentric spheres of radii ρ and R (Figure 1). The condition $\rho \leq |\mathbf{r}| \leq R$ ensures that the two grains are not overlapped. Let $\mathbf{H}_d$ be the field produced by the dipole at the origin. The amplitude H_d of $\mathbf{H}_d$ depends on the distance r of the dipole from the origin, and on the angle θ between $\mathbf{m}$ and $\mathbf{r}$:

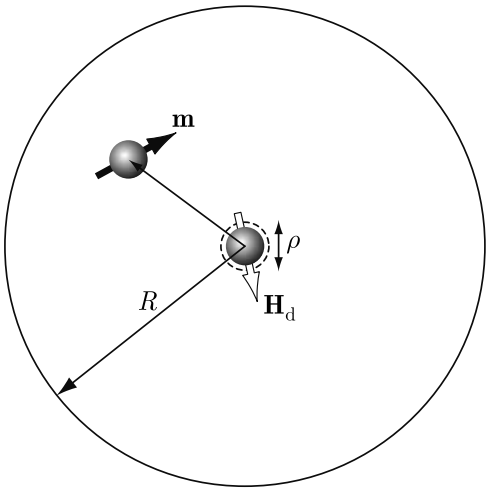

Figure 1. Geometric configuration adopted for the calculation of the interaction field (see text for notation).

$$H_d(r,\theta) = \frac{m}{4\pi r^3}\sqrt{1+3\cos^2\theta} \tag{1}$$

Being $\sin\theta$ the PDF of θ, the PDF of H_d produced by a randomly oriented dipole at a distance r is:

$$p_d(H_d|r) = \begin{cases} \dfrac{H_d}{\sqrt{3}\kappa\sqrt{H_d^2 - \kappa^2}}, & \kappa \leq H_d \leq 2\kappa \\ 0, & \text{else} \end{cases} \tag{2}$$

with $\kappa = m/(4\pi r^3)$. Consider now the projection $h = H_d\cos\lambda$ of $\mathbf{H}_d$ along a given direction (chosen to be the z axis without loss of generality). Since the angle λ between $\mathbf{H}_d$ and the z axis is random, $h = zH_d$ is the product of the random variates H_d with PDF given by (2), and $z = \cos\lambda$ with a uniform PDF p_z in the interval $[-1, +1]$. The PDF of h given r (written $h|r$) is

$$p_h(h|r) = \int_\Omega |u|^{-1} p_d(u|r) p_z(h/u)\mathrm{d}u \tag{3}$$

with $\Omega = \{u|\kappa \leq u \leq 2\kappa \bigwedge -1 \leq h/u \leq 1\}$. Integration of (3) gives

$$p_h(h|r) = \begin{cases} \dfrac{\ln(2+\sqrt{3})}{2\sqrt{3}\kappa}, & |h| \leq \kappa \\ \dfrac{\ln(2+\sqrt{3}) - \operatorname{arcosh}|h/\kappa|}{2\sqrt{3}\kappa}, & \kappa \leq |h| \leq 2\kappa \end{cases} \tag{4}$$

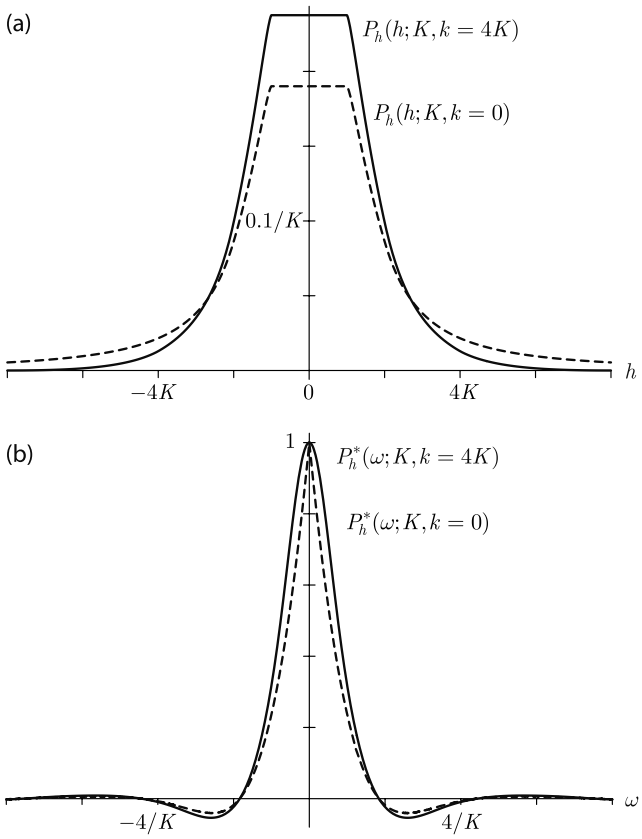

Figure 2. (a) PDF P_h of the field component along a given direction, produced by a random point dipole, when the position of the dipole is constrained within two spheres of radii $\rho < R$ (see text for notation). The solid line is the limit case $\rho = 0$; the dashed line corresponds to $R = 4\rho$. (b) Characteristic functions P_h^* of the PDFs plotted in Figure 2a. Notice that $P_h^*(\omega;\ \rho = 0)$ has a cusp at $\omega = 0$.

The probability of finding the dipole at a distance $\rho \le r \le R$ is given by the PDF $p_r(r;\ \rho,\ R) = 3r^2/(R^3 - \rho^3)$. Then, the PDF of h is

$$P_h(h) = \int_\rho^R p_h(h|r)p_r(r;\rho,R)\mathrm{d}r \tag{5}$$

with solution

$$P_h(h) = \begin{cases} \frac{\ln(2+\sqrt{3})}{4\sqrt{3}}\left(K^{-1}+k^{-1}\right), & |h| \le K \\ \frac{\ln(2+\sqrt{3})}{4\sqrt{3}}\left(K^{-1}+k^{-1}\right) + \frac{1}{8\sqrt{3}K(1-K/k)}\left[\sqrt{1-K^2/h^2} - \left(2-K^2/h^2\right)\operatorname{arcosh}\frac{h}{K}\right], & K < |h| \le 2K \\ \frac{K\ln(2+\sqrt{3})}{8\sqrt{3}(1-K/k)}\left(h^{-2}-2k^{-2}\right) + \frac{K}{4(1-K/k)h^2}, & 2K < |h| \le k \\ \frac{K\ln(2+\sqrt{3})}{8\sqrt{3}(1-K/k)}\left(h^{-2}-2k^{-2}\right) + \frac{K}{4(1-K/k)h^2} + \frac{K}{8\sqrt{3}k^2(1-K/k)}\left[\left(2-k^2/h^2\right)\operatorname{arcosh}\frac{h}{k} - \sqrt{1-k^2/h^2}\right], & k < |h| \le 2k \\ 0, & |h| > 2k \end{cases} \tag{6}$$

where $k = m/(4\pi\rho^3)$ and $K = m/(4\pi R^3)$ (Figure 2). In the limit case represented by $\rho = 0$, $P_h(h) \propto h^{-2}$ as $h \to \infty$.

2.2. Field Produced by Many Uncorrelated Random Dipoles

[10] The z component H_z of the IF produced by a collection of n dipoles is the sum of the components h of the n dipole fields. To calculate the IF produced at the place occupied by a magnetic particle in a macroscopic sample, consider following geometrical setting. The magnetic particle under consideration is sitting at the center of a coordinate system, and the sample is represented by a set of n dipoles randomly distributed and randomly oriented within a sphere of radius R. The dipoles are carried by spherical particles of diameter $\rho \ll R$. Furthermore, let p be the packing fraction of the particles, defined as the relative sample volume occupied by the particles, and N the number of particles per unit volume.

[11] The PDF of H_z is given by the n th convolution of $P_h(h)$ with itself. The convolution is best calculated in the Fourier space, where it converts to a simple product. Let $f^*(\omega)$ be the characteristic function of a PDF $f(x)$, where the asterisk denotes the Fourier transformation. Then,

$$W_{\mathrm{uc}}^*(\omega,p) = \lim_{R\to\infty}\left[P_h^*(\omega;\rho,R)\right]^n \tag{7}$$

with $n \approx 4\pi R^3 N/3 = 8pR^3/\rho^3$. The subscript "uc" is used to recall that (7) is valid in the case of completely uncorrelated dipole positions. If $n \to \infty$, the central limit theorem can be used to evaluate (7). The classic formulation of this theorem states that W_{uc} converges to a Gaussian distribution when P_h has a finite variance σ^2; a condition fulfilled by $\rho > 0$. However, the central limit theorem apply only to the central region of a PDF. In the case of (7), this region is given by $|H_z| < n^{3/4}\sigma$, because P_h is a symmetric distribution [*Sornette*, 2004]. Since $n \propto p$, it is immediately evident that the central limit theorem is not applicable in its classic formulation when $p \to 0$. This problem was avoided by *Shcherbakov and Shcherbakova* [1975] and *Berkov* [1996] by handling the two cases $p \to 0$ and $p \to 1$ separately. The drawback of this approach is the impossibility to describe intermediate cases given by $0.01 < p < 0.2$.

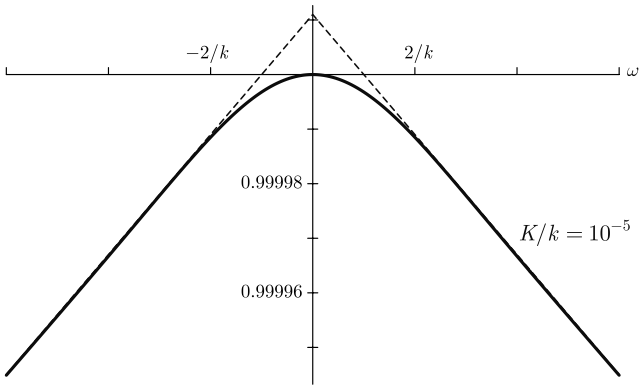

Figure 3. Detail of the characteristic function $W^*(\omega)$ showing its behavior at $\omega \to 0$.

[12] In the following, I will use a different approach, based on the properties of the characteristic function $P_h^*(\omega)$ of P_h at $\omega \to 0$. The solution of this limit is

$$\lim_{\omega\to 0} P_h^*(\omega) = 1 - \frac{p\mu_s^2}{216n}\omega^2 = 1 - \frac{\sigma_0^2\omega^2}{2n} \tag{8}$$

On the other hand, if $\rho \to 0$, P_h has the following asymptotic behavior:

$$\lim_{\rho\to 0} P_h(h \geq k) \approx \frac{p\mu_s}{12nh^2}\left[\frac{\ln(2+\sqrt{3})}{2\sqrt{3}} + 1\right] = \frac{\alpha_0}{\pi n h^2} \tag{9}$$

The power law dependence $f(x) \sim |x/a|^{-q}$ of a PDF $f(x)$ at $x \to \infty$ shapes the central region of the characteristic function $f^*(\omega)$ [*Bracewell*, 1986]. The following limit is obtained using $q = 2$:

$$\lim_{\omega\to 0} P_h^*(\omega; \rho = 0) = 1 - \frac{\alpha_0}{n}(1+\varepsilon)|\omega| \tag{10}$$

where ε is a correction factor that takes into account the approximation of (9) produced by $\rho > 0$. Since (9) is strictly valid for $\rho = 0$, $\varepsilon \to 0$ when $\rho \to 0$. The correction factor ε will be determined numerically later. Two different expressions (8) and (10) have been obtained for the central properties of $P_h^*(\omega)$. A numerical evaluation of $P_h^*(\omega)$ at $\omega \to 0$ shows that (8) holds for $|\omega| < k^{-1}$, and (10) for $|\omega| > k^{-1}$ (Figure 3). Since $k^{-1} \propto \rho^3$, and $p \propto \rho^3$ for the same configuration of dipoles, it is evident that (10) is a good approximation of the central region of $P_h^*(\omega)$ in a system characterized by $p \to 0$. On the other hand, the central limit theorem apply to (8) when $p \to 1$. Accordingly, analytical solutions of (7) can be obtained in the two limit cases of $p \to 0$ (point dipoles) and $p \to 1$. For $p \to 0$, the inverse Fourier transform of (10) is the following Lorentzian PDF:

$$\begin{aligned} W_{uc}(H_z; p, \mu_s) &= \frac{1}{\pi\alpha_0\left(1 + H_z^2/\alpha_0^2\right)} \\ \alpha_0(p, \mu_s) &= \frac{\pi p\mu_s}{12}\left[\frac{\ln(2+\sqrt{3})}{2\sqrt{3}} + 1\right] \approx 0.361 p\mu_s \end{aligned} \tag{11}$$

On the other hand, for $p \to 1$, the central limit theorem gives

$$\begin{aligned} W_{uc}(H_z; p, \mu_s) &= \frac{1}{\sqrt{2\pi}\sigma_0}\exp\left(-\frac{H_z}{2\sigma_0^2}\right) \\ \sigma_0(p, \mu_s) &= \frac{\sqrt{p/3}}{6}\mu_s \approx 0.289\mu_s\sqrt{p} \end{aligned} \tag{12}$$

For comparison, *Berkov* [1996] obtained $\alpha_0 \approx 0.36 p\mu_s$ and *Shcherbakov and Shcherbakova* [1975] calculated $\alpha_0 \approx 0.42 p\mu_s$ for randomly oriented dipoles.

[13] An analytical expression for W_{uc} cannot be found at intermediate values of p. However, the central properties (8) and (10) of W_{uc}^*, together with the fact that W_{uc} is an infinitely divisible function under the assumption of $n \to \infty$, set important constraints on the solution. Special cases of W_{uc}^* for $p \to 0$ and $p \to 1$ are exponential forms of the type $\exp(-a|\omega|)$ and $\exp(-b\omega^2)$, respectively. A suitable approximation $\tilde{W}_{uc}^*$ of W_{uc}^* is therefore chosen to be an exponential form in order to satisfy the infinite divisibility criterion. Furthermore, $\tilde{W}_{uc}^*$ should converge to (8) for $|\omega| \ll k^{-1}$ and to (10) if $|\omega| \gg k^{-1}$. An expression for $\tilde{W}^*$ that satisfies the abovementioned criteria is

$$\tilde{W}_{uc}^*(\omega) = \exp\left[\alpha\beta_{uc}^{-1} - \alpha\sqrt{\beta_{uc}^{-2} + \omega^2}\right] \tag{13}$$

with $\alpha = \alpha_0(1 + \varepsilon)$ and $\beta_{uc} = p\mu_s^2/(108\alpha)$. The correction factor $\varepsilon(p)$ is determined by comparing $W^*(\omega; p)$ and $\tilde{W}^*(\omega; p, \varepsilon)$ for different values of p and ε. The best approximation is obtained by minimizing

$$\Delta^2(p, \varepsilon) = \frac{\int_{-\infty}^{+\infty}\left[\tilde{W}_{uc}^*(\omega; p, \varepsilon) - W_{uc}^*(\omega; p)\right]^2 \mathrm{d}\omega}{\int_{-\infty}^{+\infty}\left[W_{uc}^*(\omega; p)\right]^2 \mathrm{d}\omega} \tag{14}$$

with respect to ε, whereby $W_{uc}^*(\omega; p)$ is calculated numerically using (6)–(7). The empirically determined ε is well approximated by $\varepsilon(p) = 0.359\arctan^{0.8918}(12.155p)$ (Figure 4). The maximum difference between $\tilde{W}_{uc}^*$ and W_{uc}^*

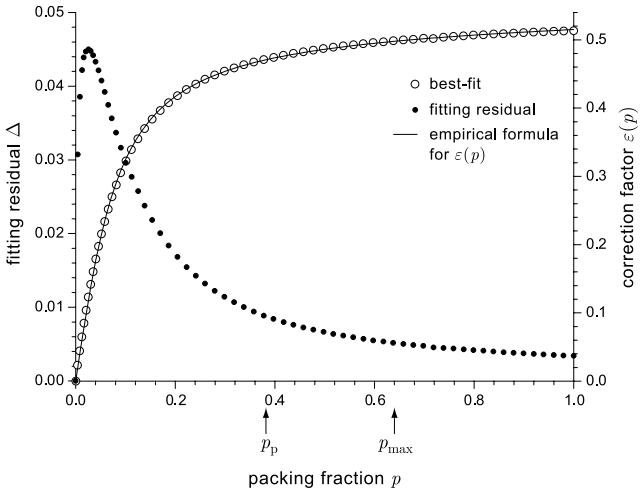

Figure 4. Empirically determined correction factor $\varepsilon(p)$ (circles) and its analytical approximation (solid line). Dots are the fitting residuals, defined by equation (14). The arrows indicate the maximum random packing fractions of spheres attainable with a Poisson process, p_p, and the physical maximum p_{max}.

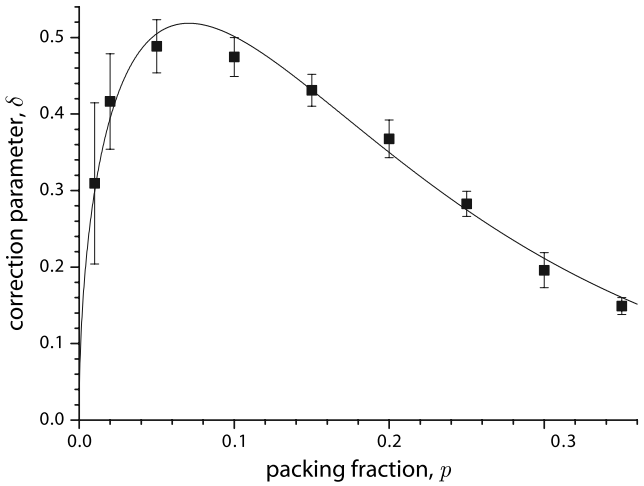

Figure 5. Empirically determined correction factor $\delta(p)$ for the spatial correlation of nonoverlapping spheres (squares). Error bars refer to the confidence intervals obtained by fitting numerically simulated sets of particles (see text). The solid line is an analytical approximation of $\delta(p)$.

occurs at intermediate values of p, however, $\Delta(p, \varepsilon) < 2.5\%$ for $0 \leq p \leq 1$. Therefore $\tilde{W}^*_{\rm uc}$ is a good approximation of $W^*_{\rm uc}$ over the entire range of p. The inverse Fourier transform of $\tilde{W}^*_{\rm uc}$ gives the PDF of H_z:

$$W_{\rm uc}(H_z; p, \mu_{\rm s}) = \frac{e^{\alpha/\beta_{\rm uc}}}{\pi\beta_{\rm uc}\sqrt{1 + H_z^2/\alpha^2}} K_1\left(\frac{\alpha}{\beta_{\rm uc}}\sqrt{1 + H_z^2/\alpha^2}\right) \tag{15}$$

where K_1 is the modified Bessel function of the second kind. The shape of W is controlled by p, since $\mu_{\rm s}$ has only a scaling effect accounted by $W_{\rm uc}(H_z; p, \mu_{\rm s}) = \mu_{\rm s}^{-1} W_{\rm uc}(H_z/\mu_{\rm s}; p, 1)$.

2.3. Field Produced by Many Nonoverlapping Random Dipoles

[14] As discussed before, the result obtained in (15) is strictly valid only if the positions of the dipoles are uncorrelated. This assumption is certainly a good approximation for systems characterized by $p \ll 1$. If a given volume is filled with N particles per unit volume at random positions, as assumed in the previous calculations, the probability P of finding exactly m particles in a volume v is given by the Poisson law: $P = (Nv)^m e^{-Nv}/m!$. If v is the volume occupied by one grain, then $p = nv$, and the overlapping probability is the probability of having $m > 1$ in a sphere of radius ρ (corresponding to a volume of $8v$). The overlapping probability is thus given by $1 - (1 + 8p)e^{-8p}$. The Lorentz approximation is practically not affected by spatial correlation effects, since, in its range of validity, the overlapping probability is <0.3%. Because the Lorentz approximation is controlled by the parameter α, it is reasonable to assume that the spatial correlation affects $\beta_{\rm uc}$. Therefore $\beta_{\rm uc}$ is replaced by $\beta = 2\beta_{\rm uc}/(1 + \delta)$, where $\delta(p)$ is determined by comparing (15) with results obtained from numerical simulations at different values of p.

[15] Numerical simulations of random assemblages of spherical particles have been performed as follows. First, spherical grains of given diameter $\rho < 1$ were randomly placed within a sphere of unit radius (random packing problem). The grains were added individually using a random number generator that simulates a Poisson process. If the newly added grain overlapped with any other grain, it was discarded, and a new grain was generated until a given value of p was reached. *Talbot et al.* [1991] calculated that the maximum packing fraction of spheres attainable by this method is $p \approx 0.382$. Since the computation time increases drastically as $p \rightarrow 0.382$, calculations were limited to $p \leq 0.35$. The maximum random packing fraction attainable with spherical grains is $p \approx 0.64$ [*Man et al.*, 2005]. However, this limit is considerably smaller when the spheres are bonded by a strong force [*Onoda and Liniger*, 1990], as it is the case with clusters of magnetic particles. The upper limit of p in clusters of magnetic particles is not known; however, A. P. Chen et al. (First-order reversal curve diagrams of natural and cultured biogenic magnetic particles, submitted to *Journal of Geophysical Research*, 2006) estimated $p < 0.35$ in clusters of single-domain (SD) particles. Therefore it can be assumed that $0 < p \leq 0.35$ is a realistic range for real samples.

[16] The packing procedure described above was used to generate 16 random assemblages of 3000 particles each with $p = 0.001, 0.002, 0.005, 0.1, 0.15, 0.2, 0.25, 0.3, 0.35$. A random number generator was then used to assign the orientation of the magnetic moment of each grain. The magnetic field produced by the 3000 randomly oriented dipoles in each assemblage was calculated at the center of the spheres, using

$$\mathbf{H}_k = \sum_{k \neq j} \frac{3\mathbf{r}_{kj}(\mathbf{r}_{kj} \cdot \mathbf{m}_j)/r_{kj}^2 - \mathbf{m}_j}{4\pi r_{kj}^3} \tag{16}$$

with $\mathbf{r}_{kj} = \mathbf{r}_j - \mathbf{r}_k$, and $m = 4\pi p/9000$ (this choice of m ensures that $\mu_{\rm s} = 1$). To avoid effects due to the finite size of the sample, the field was calculated at the center of the 12 spheres that are closest to the center of the particles assemblage. Each of the three component of $\mathbf{H}_k$ was identified with a statistical realization of H_z. The process of generating the randomly oriented magnetic moments and calculate $\mathbf{H}_k$ was repeated 6 times, giving a total of $3000 \times 12 \times 3 \times 6$ different realizations of H_z. These realizations were used to calculate the PDF of H_z with $\mu_{\rm s} = 1$. The PDF was then fitted using $W_{\rm uc}(H_z; p, 1)$, with β instead of $\beta_{\rm uc}$, by minimizing the squared residuals with respect to δ. The values of δ obtained from the minimization are well approximated by $\delta(p) = 3.2145\sqrt{p}e^{-7.067p}$ (Figure 5). The maximum difference between the numerically simulated PDF of H_z and the analytical approximation obtained from $\delta(p)$ amounts to few% (Figure 6). It can be therefore concluded that

$$\begin{aligned}
W_{\rm r}(H_z; p, \mu_{\rm s}) &= \frac{e^{\alpha/\beta}}{\pi\beta\sqrt{1 + H_z^2/\alpha^2}} K_1\left(\frac{\alpha}{\beta}\sqrt{1 + H_z^2/\alpha^2}\right) \\
\alpha(p, \mu_{\rm s}) &= \frac{\pi p\mu_{\rm s}(1 + \varepsilon)}{12}\left[\frac{\ln(2 + \sqrt{3})}{2\sqrt{3}} + 1\right], \\
\beta(p, \mu_{\rm s}) &= \frac{p\mu_{\rm s}^2}{54\alpha(1 + \delta)} \\
\varepsilon(p) &= 0.359\arctan^{0.8918}(12.155p), \quad \delta(p) = 3.2145\sqrt{p}e^{-7.067p}
\end{aligned} \tag{17}$$

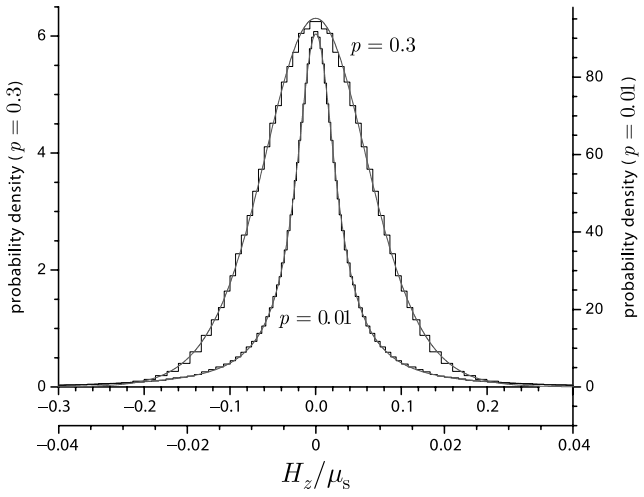

Figure 6. Numerically simulated PDFs of the local IF (stepped lines) and the corresponding analytical expression given by equation (17) (solid line), for $p = 0.01$ and $p = 0.3$, respectively.

is a suitable analytical expression for the PDF of H_z. The subscript "r" is used to remind that this solution is valid for the case of randomly oriented dipoles. A comparison of W_r for different values of p determines the validity range of the limit cases (11)–(12) (Figure 7). The Lorentz approximation (11) apply reasonably well in for $0 < p \leq 0.01$; on the other hand, the Gaussian approximation (12) is valid for $p \geq 0.2$. An intermediate situation is obtained for $p \approx 0.05$.

3. Interaction Field of Nonrandomly Oriented Dipoles

[17] A set of randomly oriented uniaxial particles subjected to an external field H along the z axis will have a distribution of moment orientations that depends on H and on the magnetization state. The moments are preferentially aligned with H if the magnetization is positive. On the other hand, the magnetic moments of particles that are about to switch tend to flatten on the xy plane. The general case is intermediate between three idealized situations given by (1) randomly oriented dipoles, already solved in section 2, (2) perfectly aligned dipoles, and (3) dipoles at a right angle to the applied field, which I will shortly call perpendicular dipoles. Cases 2 and 3 can be solved in a similar way as case 1. Case 2 is solved analytically in strict analogy with section 2, and the following PDF is obtained for the local IF produced by aligned dipoles:

$$W_a(H_z;p,\mu_s) = \frac{e^{\alpha/\beta}}{\pi\beta\sqrt{1+H_z^2/\alpha^2}} K_1\left(\frac{\alpha}{\beta}\sqrt{1+H_z^2/\alpha^2}\right)$$
$$\alpha(p,\mu_s) = \frac{\pi p\mu_s(1+\varepsilon)}{4\sqrt{3}}\ , \quad \beta(p,\mu_s) = \frac{p\mu_s^2(1+\delta)}{400\alpha}$$
$$\varepsilon(p) = 0.359\arctan^{0.8918}(12.155p)\ , \quad \delta(p) = 17.90\sqrt{p}e^{-8.458p} \tag{18}$$

where $\varepsilon(p)$ is the same as in (17), and $\delta(p)$ was determined by comparison of the analytical expression with the numerical results. The PDFs for aligned and randomly oriented dipoles are similar in shape, however, the width of the two functions is different, especially for $p > 0.1$ (Figure 8). A similar result was found by *Berkov* [1996] for the variance of the local IF. He explained this difference in terms of two contributions to the IF variance related to the spatial arrangement of the particles on one hand, and to the orientation of the dipoles on the other. As the density of the particle assemblage increases, the local IF is determined mainly by neighbor particles in the first coordination sphere. As $p \rightarrow 0.6$, the local structure converges to a hexagonal lattice. If the magnetic moments of the resulting short-range ordered configuration are aligned, the IF variance is determined mainly by the small contribution of long-range interactions.

[18] The case of perpendicular dipoles cannot be solved analytically. The analogon of equation (6) was calculated

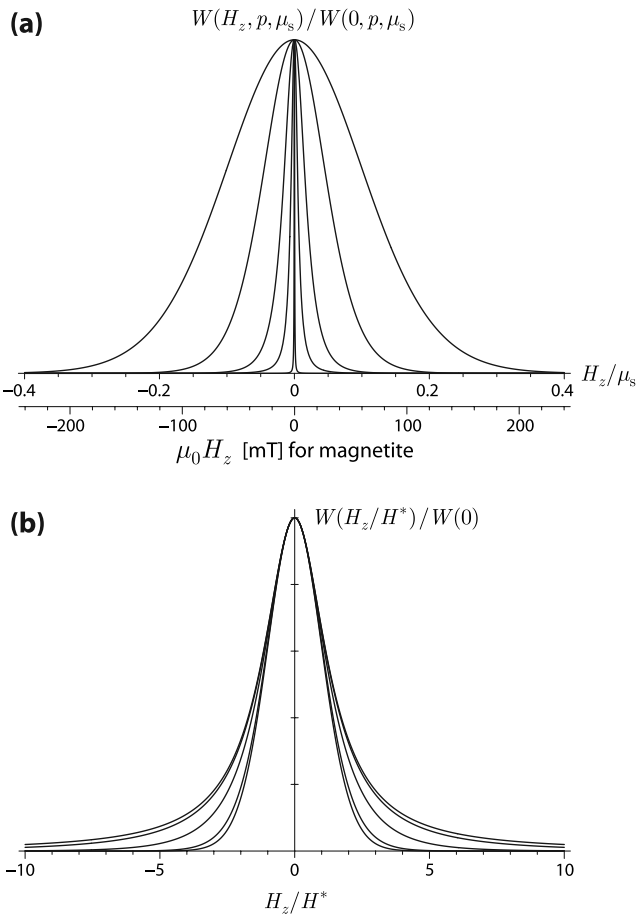

Figure 7. (a) The PDF of the local IF along a given direction, produced by a random assemblages of magnetic particles with packing fractions p of 0.001, 0.015, 0.05, 0.2, 0.64, respectively (from the center of the plot toward outside). The second abscissa represents the IF of magnetite particles. All PDFs have been normalized to unit at $H_z = 0$. (b) For better visualization of the differences in shapes at various values of p, the field axis has been rescaled for each curve, so that all PDFs are identical at $H_z = 0$. Notice that the case of $p = 0.05$ is intermediate between the Gaussian limit, valid for $p > 0.2$, and the Lorentz limit, valid for $p < 0.015$.

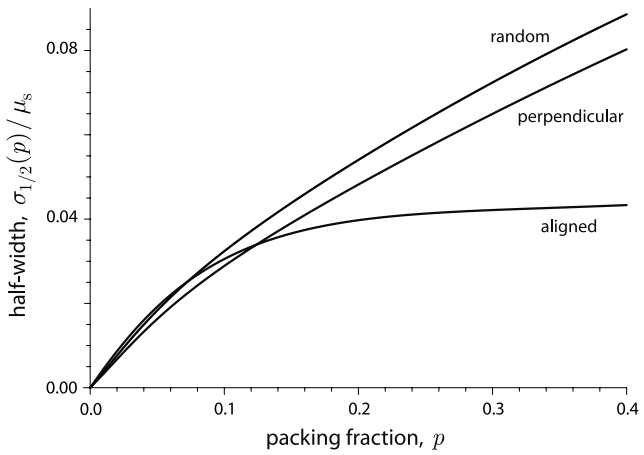

Figure 8. Half width $\sigma_{1/2}$ of the IFD produced by magnetic dipoles that are randomly oriented, aligned, and perpendicular to a given direction, respectively.

numerically, whereby the asymptotic behavior of P_h and its variance were used to calculate the coefficients α and β. The generalization of P_h for the case of many particles is the same as described in section 2, and gives the following PDF for the local interaction field of perpendicular dipoles:

$$W_p(H_z;p,\mu_s)=\frac{e^{\alpha/\beta}}{\pi\beta\sqrt{1+H_z^2/\alpha^2}}K_1\left(\frac{\alpha}{\beta}\sqrt{1+H_z^2/\alpha^2}\right)$$
$$\alpha(p,\mu_s)=0.3175p\mu_s(1+\varepsilon)\ ,\quad \beta(p,\mu_s)=0.01664\frac{p\mu_s^2}{\alpha(1+\delta)}$$
$$\varepsilon(p)=0.359\arctan^{0.8918}(12.155p)\ ,\quad \delta(p)=3.868\sqrt{p}e^{-6.098p} \tag{19}$$

The IF produced by perpendicular dipoles is similar to that of random dipoles (Figure 8). A concentration-independent relative difference of 14% between the two cases is produced by the different values of α in (17) and (19).

[19] For the practical purpose of estimating p from the width of the IFD, W_r and W_p can be considered identical. In the following I consider the case of partially aligned moments, which I will describe using the parameter $\gamma = |M|/M_s$. The special cases of randomly oriented and totally aligned dipoles are given by $\gamma = 0$ and $\gamma = 1$, respectively. The IF of intermediate cases can be imagined as the weighted superposition of two contributions produced by perfectly aligned dipoles with magnetic moment $\mu_z = z\mu_s$ on one hand, and random dipoles with magnetic moment $\mu_r = r\mu_s$ on the other. Each normalized moment $\mathbf{u}$ can be decomposed into a randomly oriented component $\mathbf{R}$ at an angle φ with respect to the z axis, and a component $\mathbf{Z}$ parallel to the z axis. Since $|\mathbf{u}| = 1$,

$$Z(\varphi)=\sqrt{1-R^2\sin\varphi}-R\cos\varphi \tag{20}$$

Integration over all angles φ gives

$$z=\int_0^{\pi/2}Z(\varphi)\sin\varphi d\varphi=\frac{1-r}{4r}\left[(1+r)\ln\frac{1+r}{1-r}+2r\right] \tag{21}$$

Since $\gamma = z$, $r(\gamma)$ is obtained from a numerical solution of (21). A good analytical approximation of the solution is $r \approx (1 - \gamma^{1.37})^{0.834}$. The difference between the random and the aligned case is controlled by the parameter β. Since the variances of W_r and W_a at $p \to 1$ are proportional to β, the IFD of partially aligned dipoles is given by $W(H_z; p, \mu_s)$ with:

$$\alpha(\gamma)\approx\alpha_r$$
$$\beta(\gamma)\approx(1-\gamma^{1.37})^{1.67}\beta_r+\gamma^2\beta_a \tag{22}$$

where the subscripts "r" and "a" refer to the solutions for random dipoles and aligned dipoles, respectively.

4. FORC Functions of Interacting SD Particles

[20] Preisach diagrams [*Preisach*, 1935] provide information about the statistical distributions of switching fields and interaction fields in a sample. *Néel* [1954], proposed a simple interpretation of the Preisach function $F(H_c \geq 0, H_u)$ as the PDF of the contributions of elemental squared hysteresis loops with switching fields $H_a = H_u - H_c$ and $H_b = H_u + H_c$. In the case of SD particles, H_c and H_u would have the physical meaning of a coercivity and a IF, respectively. In the basic Preisach model, it is further assumed that the IF is independent of the magnetization state of the sample, a restriction formalized by $F(H_c, H_u) = f(H_c)g(H_u)$, where $f(H_c)$ and $g(H_u)$ are the PDFs of the switching fields and the IFs, respectively [*Pike et al.*, 1999]. This result is particularly appealing, because $F(H_c, H_u)$ would provide a direct measurement of the IFD, from which the packing density of the particles could be estimated using equations (17)–(19). However, the assumptions of the basic Preisach model are unrealistic, as proved by numerical simulations of densely packed SD particles [e.g., *Stancu et al.*, 2001; *Cerchez et al.*, 2004]. Modifications of the classic Preisach model such as the moving Preisach model [*Della Torre*, 1965; *Hejda and Zelinka*, 1990], and the variable variance Preisach model [*Pardavi-Horvath et al.*, 1993] have been suggested as better models for real samples.

[21] FORCs provide an attractive method of determining the Preisach distribution that has gained popularity in recent years [e.g., *Pike et al.*, 1999; *Roberts et al.*, 2000]. The FORC distribution $\rho(H_c, H_u)$ of interacting SD particles shares some common characteristics with the classic Preisach model. For example, measurements [*Pike et al.*, 1999; *Carvallo et al.*, 2005] and numerical models [*Muxworthy and Williams*, 2005] of interacting SD particles show that the width of the FORC distribution along H_u increases with increasing packing fraction, as predicted by the classic Preisach model. On the other hand, the measurement of FORC and Preisach diagrams of SD particles as a function of temperature gave contradictory results that raise some questions on the interpretation of the dispersion along H_u as a measure of the interaction strength [*Dunlop et al.*, 1990; *Carvallo et al.*, 2004]. FORC distributions of SD assemblages are characterized by distinct features, such as regions characterized by negative values, that depend on the asymmetric measurement procedure of FORCs and on intrinsic properties of SD grains [*Muxworthy et al.* 2004; *Newell*,

2005]. It is therefore questionable whether $\rho(H_c, H_u)$ effectively represents a statistical distribution of coercivities and interaction fields in a sample of SD particles.

[22] Detailed numerical simulations of high-density three-dimensional arrays of SD particles ($p > 0.13$), suggest a collapse of $\rho(H_c, H_u)$ as the particle distance becomes smaller than the particle's diameter [*Muxworthy et al.*, 2004]. It is not clear whether the collapse of the FORC distribution is (1) an artifact of the numerical algorithm used in the micromagnetic calculation, (2) a consequence of the highly ordered configuration of identical, cubic three-dimensional arrays of particles, or (3) an intrinsic property of high-density particle systems. Efficient fast Fourier transform (FFT) algorithms used for these simulations require the particles to be placed on a regular grid, and the direct calculation of random particle assemblages using equation (16) is too slow for FORC calculations. Therefore approximated analytical modes for the FORC distribution of random assemblages of SD particles are developed in the following in order to test the possibility of a quantitative interpretation of $\rho(H_c, H_u)$.

4.1. Classic Basic Preisach Model

[23] A FORC is measured by saturating the sample in a large positive field, which is then decreased to a reversal field H_a. The magnetization measured at a successive applied field $H_b \geq H_a$ is denoted by $M(H_a, H_b)$. The FORC distribution is defined as

$$\rho = -\frac{\partial^2 M}{\partial H_a \partial H_b} = \frac{1}{4}\left(\frac{\partial^2 M}{\partial H_c^2} - \frac{\partial^2 M}{\partial H_u^2}\right) \tag{23}$$

[*Pike et al.*, 1999]. The simplest physical model of FORCs, called the basic Preisach model, identify $M(H_a, H_b)$ with the contribution of elemental squared hysteresis loops under the influence of a fixed IF [*Pike et al.*, 1999]. According to this model,

$$M(H_a, H_b) = 1 - 2\int_0^\infty f(H)\mathrm{d}H \int_{-\infty}^{\min[-H-H_a, H-H_b]} g(H_i)\mathrm{d}H_i \tag{24}$$

and the derivative of (24) is $f(H_c)g(H_u)$. As noted by *Mayergoyz* [1991], the Preisach model is a mathematical representation of hysteresis that does not account for the fact that the IF depends on the magnetization state. An exact model of FORCs has been calculated by *Newell* [2005] for noninteracting Stoner-Wohlfarth (S-W) particles.

[24] A realistic model for interacting SD particles must account for (1) the reversible magnetization produced by moment rotation in a field, (2) the dependence of the IFD on the overall statistical alignment of the moments, and (3) the fact that the local interaction field acting on a given particle changes during the measurement of a FORC. These effects are extremely difficult to account for, however, simplified analytical solutions for the limit case of weakly interacting systems will be provided in the following.

4.2. IF in FORC Models: From Vectors to Scalars

[25] The basic Preisach model assumes that the interaction field acting on a given particle does not change when the field is ramped from H_a to H_b. It is easy to show that this assumption is not valid, since the orientation of the magnetic moments in H_a and H_b is different if $H_b \neq H_a$. Given the magnetic moment $\mathbf{m}$ of a particle, the two orthogonal vectors

$$\begin{aligned} \mathbf{w} &= \frac{1}{2}[\mathbf{m}(H_b) + \mathbf{m}(H_a)] \\ \mathbf{s} &= \frac{1}{2}[\mathbf{m}(H_b) - \mathbf{m}(H_a)] \end{aligned} \tag{25}$$

represent the constant and the changing component of $\mathbf{m}$, since $\mathbf{m}(H_a) = \mathbf{w} - \mathbf{s}$ and $\mathbf{m}(H_b) = \mathbf{w} + \mathbf{s}$. In a large set of particles, the IF at any point is the sum of the contribution from all the $\mathbf{w}$ and $\mathbf{s}$ vectors. Since $\mathbf{w}$ and $\mathbf{s}$ are orthogonal and contained in randomly oriented planes, the corresponding contributions to the total IF are uncorrelated. Therefore the total IFD is given by the convolution of the IFDs produced by the $\mathbf{w}$ and $\mathbf{s}$ vectors. The scaling property $W(H, a\mu_s) = a^{-1}W(a^{-1}H, \mu_s)$ allows to model the IFs produced by the $\mathbf{w}$ and $\mathbf{s}$ vectors as the total IF multiplied by the average modules w and s normalized by $|\mathbf{m}|$. Using the cosine theorem,

$$\begin{aligned} w &= \frac{1}{N|\mathbf{m}|}\sum_{k=1}^{N}|\mathbf{w}_k| = \sum_{k=1}^{N} J_+\left(\theta_{b,k} - \theta_{a,k}\right) \\ s &= \frac{1}{N|\mathbf{m}|}\sum_{k=1}^{N}|\mathbf{s}_k| = \sum_{k=1}^{N} J_-\left(\theta_{b,k} - \theta_{a,k}\right) \end{aligned} \tag{26}$$

where $2J_\pm(x) = \sqrt{2 \pm 2\cos x}$, and $\theta_{a,k}$, $\theta_{b,k}$ are the angles between the magnetic moments in H_a and H_b and the applied field. The total fields acting in H_a and H_b can then be written as

$$\begin{aligned} \mathbf{h}_a &= \mathbf{H}_a + w\mathbf{H}_w - s\mathbf{H}_s \\ \mathbf{h}_b &= \mathbf{H}_b + w\mathbf{H}_w + s\mathbf{H}_s \end{aligned} \tag{27}$$

where $\mathbf{H}_w$ and $\mathbf{H}_s$ are two uncorrelated statistical realizations of random variates that represent the IF produced by the $\mathbf{w}$ and the $\mathbf{s}$ vectors, respectively. Equation (27) correctly represents the statistical relationship between the IFs at H_a and H_b as it can be easily verified for the limit cases given by $H_b = -H_a \to \infty$, (the IFs are opposite), and $H_b \to H_a$ (the IFs are identical).

[26] The next problem is related to the fact that the random orientation of the IF violates the symmetry of the equations governing noninteracting Stoner-Wohlfarth particles. A strict solution would require the evaluation of multiple vector integrals over the numerical solution of quartic equations, which is computationally very slow [*Mayergoyz*, 1991]. Therefore I will introduce a simplification for the case of weak interactions that allows to consider the IF as a scalar stochastic variate. To do so, I introduce the IF vector $h_i = [\sin\lambda\cos\psi, \sin\lambda\sin\psi, \cos\lambda]$ in spherical coordinates (λ, ψ), and I define the case of weak interactions by $h_i \to 0$. If $\mathbf{H}$ is an external applied field at an angle φ to the easy axis of a given particle, $\mathbf{H}^* = \mathbf{H} + \mathbf{h}_i$ is the total field acting on the particle's moment, and $\varphi^* = \varphi + \delta\varphi$ is its

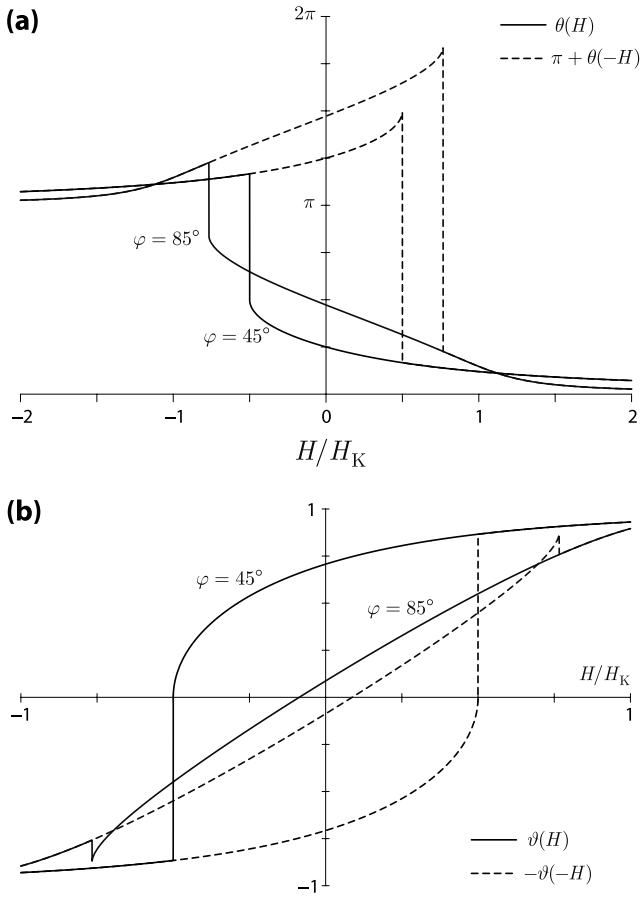

Figure 9. (a) The angle θ of S-W particles at equilibrium in a field H, and (b) the component $\vartheta = \cos\theta$ of the magnetic moment along H. Solid lines refer to the upper branch of the hysteresis loop; dashed lines refer to the lower branch. Two examples for particles whose easy axes are at $\varphi = 45°$ and $\varphi = 85°$ to the applied field are shown.

angle to the easy axis. If $h_i \ll H$, simple trigonometry gives $\delta\varphi(H) \approx \sin\lambda\cos\psi h_i/H$. Since FORCs of SD particles are strongly controlled by moment switching, I consider the difference δh_{sw} between the switching fields H_{sw} obtained by applying an external field with and without considering $\mathbf{h}_i$. Using the chain rule of derivatives, the expected value of δh_{sw}^2 for randomly oriented particles is given by

$$\langle \delta h_{sw}^2 \rangle = \frac{h_i^2}{4\pi}\int_{\lambda=0}^{\pi}\int_{\psi=0}^{2\pi}\int_{\varphi=0}^{\pi/2}\left[\cos\lambda + \frac{\partial_\varphi H_{sw}}{H_{sw}}\sin\lambda\cos\psi\right]^2 \sin\varphi \mathrm{d}\varphi\mathrm{d}\lambda\mathrm{d}\psi \tag{28}$$

If the particles reverse by coherent rotation, a numerical integration of (28) using the *Stoner and Wohlfarth* [1948] solution for $H_{sw}(\varphi)$ gives $\langle \delta h_{sw}^2 \rangle \approx 0.72 h_i^2$. Other reversal modes give slightly different results: for example, $\langle \delta h_{sw}^2 \rangle \approx 0.98\ h_i^2$ for curling reversals calculated by *Aharoni* [1999].

[27] The one-dimensional case is obtained by comparing (28) with the result obtained by considering only the component h_z of $\mathbf{h}_i$ parallel to the applied field. In this case, $\langle \delta h_{sw}^2 \rangle_z \approx 0.39\ h_i^2$, independently of the reversal mechanism. The effect of all three components of $\mathbf{h}_i$ on the moment switching is thus equivalent to that of h_z multiplied by a factor $\zeta = \langle \delta h_{sw}^2 \rangle^{1/2}/\langle \delta h_{sw}^2 \rangle_z^{1/2}$, whereby $\zeta \approx 1.354$ for Stoner-Wohlfarth particles, and $\zeta \approx 1.58$ for curling reversal modes. This result allow to replace the three-dimensional IF by a scalar field with PDF $W(H, p, \zeta\mu_s)$, provided that the typical amplitude of the IF is much smaller than the switching fields. A similar straightforward simplification is not possible in case of strong interactions, where the anisotropy of the particles is strongly modified by the IF.

[28] In the following, I limit all the calculation to the case of weak interactions described above. In this case, all vectors in equation (27) can now be replaced by scalars, whereby $g_w(x) = W(x, p, \zeta\mu_s, \gamma_w)$ and $g_s(x) = W(x, p, \zeta\mu_s, \gamma_s)$ are the PDFs of the random variates H_w and H_s, respectively.

4.3. General FORC Equations for Weak Interactions

[29] Consider a set of noninteracting particles with FORC end points given by the magnetizations $K_a = K(H_a)$ and $K_b = K(H_b)$. The interacting case is obtained by placing the same particles at random positions within a finite volume, whereby the resulting total fields h_a and h_b are defined by equation (27). The total magnetizations $M_a = M(H_a)$ and $M_b = M(H_b)$ are obtained by weighted integration of K_a and K_b over all possible values of the IF:

$$\begin{aligned} M_a &= \int_{-\infty}^{\infty}\int_{-\infty}^{\infty} g_w(x)g_s(y)K_a\left(H_a' + wx - sy\right)\mathrm{d}x\mathrm{d}y \\ M_b &= \int_{-\infty}^{\infty}\int_{-\infty}^{\infty} g_w(x)g_s(y)K_b\left(H_a' + wx - sy, H_b' + wx + sy\right)\mathrm{d}x\mathrm{d}y \end{aligned} \tag{29}$$

with $H_a' = H_a - DM_a$ and $H_b' = H_b - DM_b$, where D is a constant factor that accounts for the mean value of the interaction field. In isotropic samples, D coincides with the demagnetizing factor. Equation (29) provides a general solution for the FORCs of weakly interacting particles. It should be noted that (29) is an implicit equation, since w and s depend on the magnetization states in H_a and H_b.

[30] I will now derive a particular case of (29) for SD particles with antisymmetric elemental hysteresis loops. Such loops are uniquely described by an upper branch $\vartheta^+(H)$, obtained by decreasing the field from positive saturation, and a lower branch $\vartheta^-(H)$ obtained by increasing the field from negative saturation. The loop is antisymmetric if $\vartheta^-(H) = -\vartheta^+(-H)$, and I call it elemental if the magnetization always coincides with one of the two branches, regardless of the magnetic treatment. Two examples of such loops are given by Stoner-Wohlfarth particles (Figure 9), and by the rectangular hysteresis operator $\hat{\gamma}_{\alpha\beta}$ of the Preisach model [*Mayergoyz*, 1991]. In the case of Stoner-Wohlfarth particles, $\vartheta = \vartheta(H/H_K, \varphi)$ depend on the ratio of the field to the microcoercivity H_K of the particle, and on the angle φ of the easy axis to the applied field. On the other hand, $\vartheta(H) \equiv 1$ describes a rectangular loop in the classic Preisach model. If $H_{sw}(\varphi)$ is the switching field, $\vartheta = \vartheta(H > H_{sw}, \varphi)$ is a continuous and derivable function, and each elemental hysteresis loops can be expressed using $\vartheta(H)$ in the range $[H_{sw}, \infty]$.

[31] A large set of identical, randomly oriented Stoner-Wohlfarth particles with microcoercivity distribution $f(H_K)$ will thus have a magnetization

$$M_\beta = \int_0^\infty f(H_K)\mathrm{d}H_K \int_0^{\pi/2} \sin\varphi \mathrm{d}\varphi \cdot \int_{-\infty}^{\infty}\int_{-\infty}^{\infty} S_\beta g_w(x) g_s(y) \vartheta\left(S_\beta h_\beta / H_K\right)\mathrm{d}x\mathrm{d}y \quad (30)$$

where $\beta \equiv$ a or $\beta \equiv$ b, and $S = \pm 1$ is the switching state of a particle in H_a or H_b. Equation (30) has some similarities with the expression derived by *Mayergoyz* [1991] in his geometric interpretation of the Preisach model. The calculation of w and s requires knowledge of the angle $\theta(H/H_K, \varphi)$ of the magnetic moments at equilibrium. If $\theta(H/H_K, \varphi)$ describes the equilibrium angle on the upper branch of the elemental loop, the angle on the lower branch is $\pi + \theta(-H/H_K, \varphi)$ (Figure 9). Using (26),

$$w, s = \int_0^\infty f(H_K)\mathrm{d}HK \int_0^{\pi/2} \sin\varphi \mathrm{d}\varphi \times \int_{-\infty}^{\infty}\int_{-\infty}^{\infty} g_w(x) g_s(y) \cdot J_{\pm S_a S_b}[\theta(S_b h_b/H_K) - \theta(S_a h_a/H_K)]\mathrm{d}x\mathrm{d}y \quad (31)$$

where the "+" and the "−" cases apply to w and s, respectively. A careful analysis of the possible switching states of all particles in H_a and H_b gives the following integration limits for x and y:

$$\begin{aligned}\iint_{x,y} = &+ \int_{x=-H_{sw}-H'_u}^{\infty}\int_{y=-H_{sw}-H'_b-x}^{H_{sw}+H'_a+x} (\uparrow\uparrow) \\ &+ \int_{x=-\infty}^{-H'_u}\int_{y=H_{sw}-H'_b-x}^{\infty} + \int_{x=-H'_u}^{\infty}\int_{y=H_{sw}+H'_a+x}^{\infty} (\downarrow\uparrow) \\ &+ \int_{x=-\infty}^{-H_{sw}-H'_u}\int_{y=-\infty}^{H_{sw}+H'_a+x} + \int_{x=-H_{sw}-H'_u}^{\infty}\int_{y=-\infty}^{-H_{sw}-H'_b-x} (\uparrow\downarrow) \\ &+ \int_{x=-\infty}^{-H'_u}\int_{y=H_{sw}+H'_a+x}^{H_{sw}-H'_b-x} (\downarrow\downarrow) \end{aligned} \quad (32)$$

with $H'_u = (H'_a + H'_b)/2$, and the arrows indicating the possible combinations of switching states (positive: ↑, negative: ↓) in H_a (first arrow) and H_b (second arrow).

[32] Equations (30)–(32) can be solved iteratively starting from any initial condition $0 < w < 1$ and $0 < s < 1$ to obtain the magnetization in H_b and the corresponding FORC distribution. Each of the six integrals in (32) has a continuous argument, however, its derivative diverges at one integration limit, if this limit coincides with the switching field. Since the numerical evaluation of (30)–(32) involves four-dimensional integrals of functions that are pathological at one integration limit, the calculation of FORCs is computationally very slow. The typical computation time on a up-to-date personal computer amounts to more than five hours for one $\{H_a, H_b\}$ pair. In the following, I will show how a further simplification of (30)–(32) gives a simple result for the FORC function.

4.4. FORC Function of Weakly Interacting SD Particles

[33] The mixed derivative of (30) is complicated by the dependence of w and s on the FORC coordinates. In assemblages of noninteracting, randomly oriented S-W particles with microcoercivity H_K, $w(H_c, H_u)$ and $s(H_c, H_u)$ are characterized by cusps that are located in the lower half of the FORC space if $2H_c < H_K$, or at $H_u = 0$ if $2H_c \geq H_K$ (Figure 10b). These cusps give raise to infinite mixed derivatives that are responsible for the diverging parts of the FORC function calculated by *Newell* [2005]. If a broad distribution $\kappa(H_K)$ of microcoercivities is assumed for the previously described S-W particle assemblage, w and s become nearly even functions of H_u with a cusp in $H_u = 0$ (Figure 10d). The maximum amplitude of the partial derivatives is inversely proportional to both the median μ_K and the dispersion σ_K of $\kappa(H_K)$. According to (31), w and s for the interacting case are obtained by convolution of the noninteracting solutions with the IFD. The convolution operation eliminates the cusp at $H_u = 0$ and generates a finite second derivative that is inversely proportional to μ_K and σ_K. If the typical amplitude of the IF is much smaller than μ_K and σ_K, all first- and second-order derivatives of w and s can be neglected in the calculation of the FORC diagram. Therefore I will limit the following calculation of the FORC function the case of weak interactions, rigorously defined by $\sigma_i \ll \mu_K$ and $\sigma_i \ll \sigma_K$, where σ_i is the width if the IFD. At this point, it is convenient to introduce the switching field distribution $f(H_{sw})$ and the cumulative function $F(H_{sw})$

$$\begin{aligned} f(H_{sw}) &= \int_0^{\pi/2} \kappa[H_{sw}/h_{sw}(\varphi)]\sin\varphi \mathrm{d}\varphi \\ F(H_{sw}) &= \int_{H_c}^{\infty} f(H_{sw}) \end{aligned} \quad (33)$$

where $h_{sw} = H_{sw}/H_K$ is the angular dependence of the switching field. In the case of weak interactions defined above, w and s are practically independent of H_u in the region where the FORC function is not zero. If the elemental loops are perfectly squared, the approximated solution of (31) is $s = 1 - w$ with $w(H_c) = F(H_c)$. A slightly different result is obtained in the case of S-W particles (Figure 10c).

[34] The mixed derivative of (30) obtained by neglecting the derivatives of w and s gives the following FORC function for $H_c \gg \sigma_i$:

$$\begin{aligned} \rho(H_c, H_u) &= P + Q \\ P &= \frac{1}{ws}\int_0^\infty \kappa(H_K)\mathrm{d}H_K \int_0^{\pi/2} \bar{\vartheta}(h_{sw}) g_w\left(\frac{H'_u}{w}\right) g_s\left(\frac{H_{sw} - H'_c}{s}\right)\sin\varphi \mathrm{d}\varphi \\ Q &= \frac{1}{ws}\int_0^\infty \kappa(H_K)\mathrm{d}H_K \int_0^{\pi/2} \sin\varphi \mathrm{d}\varphi \cdot \int_0^{H_{sw}} g_w\left(\frac{x + H'_u}{w}\right) g_s\left(\frac{H_{sw} - H'_c - x}{s}\right)\Delta\vartheta'(2x/H_K - h_{sw})\mathrm{d}x \end{aligned} \quad (34)$$

with $\bar{\vartheta}(x) = [\vartheta(x) + \vartheta(-x)]/2$, $\Delta\vartheta(x) = \vartheta(x) - \vartheta(-x)$, and $\vartheta'(x) = \partial_x\vartheta(x)$. This result can be further simplified using the condition $\sigma_i \ll \sigma_K$, which allow to consider g_w and g_s as Dirac δ functions. Furthermore, the demagnetizing field is negligible in weakly interacting systems, and H'_c and H'_u can

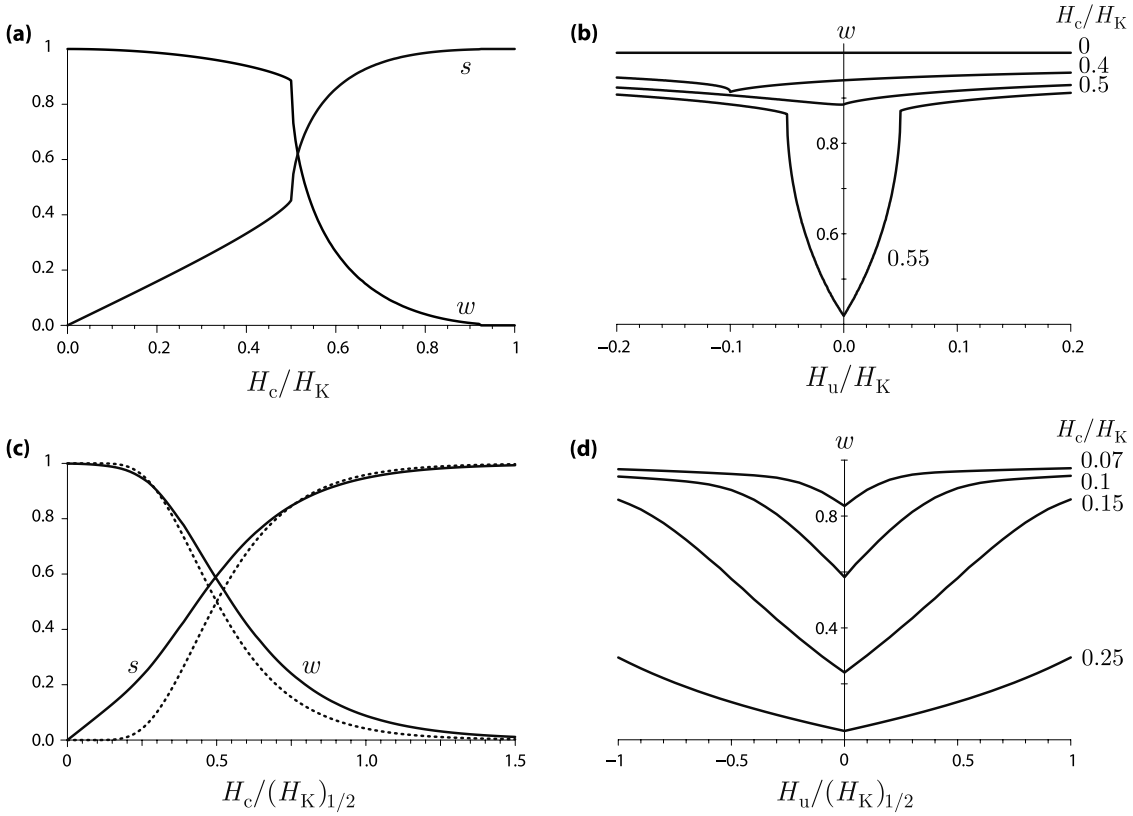

Figure 10. (a) The parameters $w(H_c, 0)$ and $s(H_c, 0)$ and (b) $w(H_c, H_u)$ for various H_c values, calculated for a set of identical, noninteracting, randomly oriented S-W particles. (c, d) Same as Figures 10a and 10b, for a set of randomly oriented S-W particles with a distribution of microcoercivities given by a logarithmic Gaussian function with median $(H_K)_{1/2}$ and dispersion parameter $\sigma = 0.4$. Dotted lines in Figure 10c corresponds to the cumulative coercivity distribution $F(H_c)$, and $1 - F(H_c)$, respectively.

be replaced by the corresponding FORC coordinates. This lead to a further simplification of P:

$$P \approx \frac{\langle \bar{\vartheta}_{sw} \rangle}{w} f(H_c) g_w\left(\frac{H_u}{w}\right) \tag{35}$$

where $\langle \bar{\vartheta}_{sw} \rangle$ is the weighted average of $\bar{\vartheta}(h_{sw})$ over all angles. Randomly oriented S-W particles are characterized by $\langle \bar{\vartheta}_{sw} \rangle \approx 0.542$; on the other hand, $\langle \bar{\vartheta}_{sw} \rangle = 1$ in the case of rectangular loops.

[35] I will now discuss the physical meaning of the terms P and Q in the $\{H_c, H_u\}$ space. The first term, P, coincides with a Preisach function if w does not depend on H_c, however, this is never the case for coercivity distributions with a finite median (Figure 10c). The width σ_u of P along H_u is proportional to w, which represents the constant part of all magnetic moments through the endpoints of a FORC defined by $\{H_c, H_u\}$. Since $\partial w/\partial H_c < 0$, σ_u decreases monotonically toward the right end of the FORC space. The same feature is observed in short-range interacting systems and was called "completion symmetry" by *Pike et al.* [2005]. The integral of P over the FORC space, called normalization integral, is equal to $\langle \bar{\vartheta}_{sw} \rangle$, whereby $\langle \bar{\vartheta}_{sw} \rangle = 1$ only for particles with squared hysteresis loops. In all other cases, the reversible part of the hysteresis loops lowers the normalization integral, as noted by *Pike* [2003].

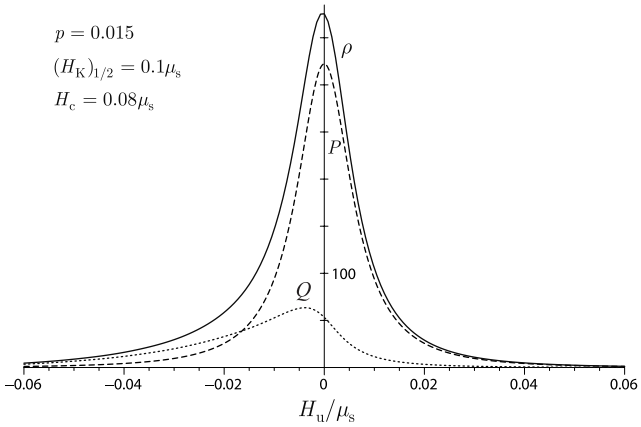

Figure 11. The two contributions P (dashed line) and Q (dotted line) of the FORC function ρ (solid line) for an interacting assemblage of randomly oriented S-W particles with packing fraction $p = 0.015$ and a distribution of microcoercivities given by a logarithmic Gaussian function with median $(H_K)_{1/2} = 0.2\mu_s$ and dispersion parameter $\sigma = 0.4$. A profile of the FORC function through $H_c = 0.08\mu_s$ is shown here.

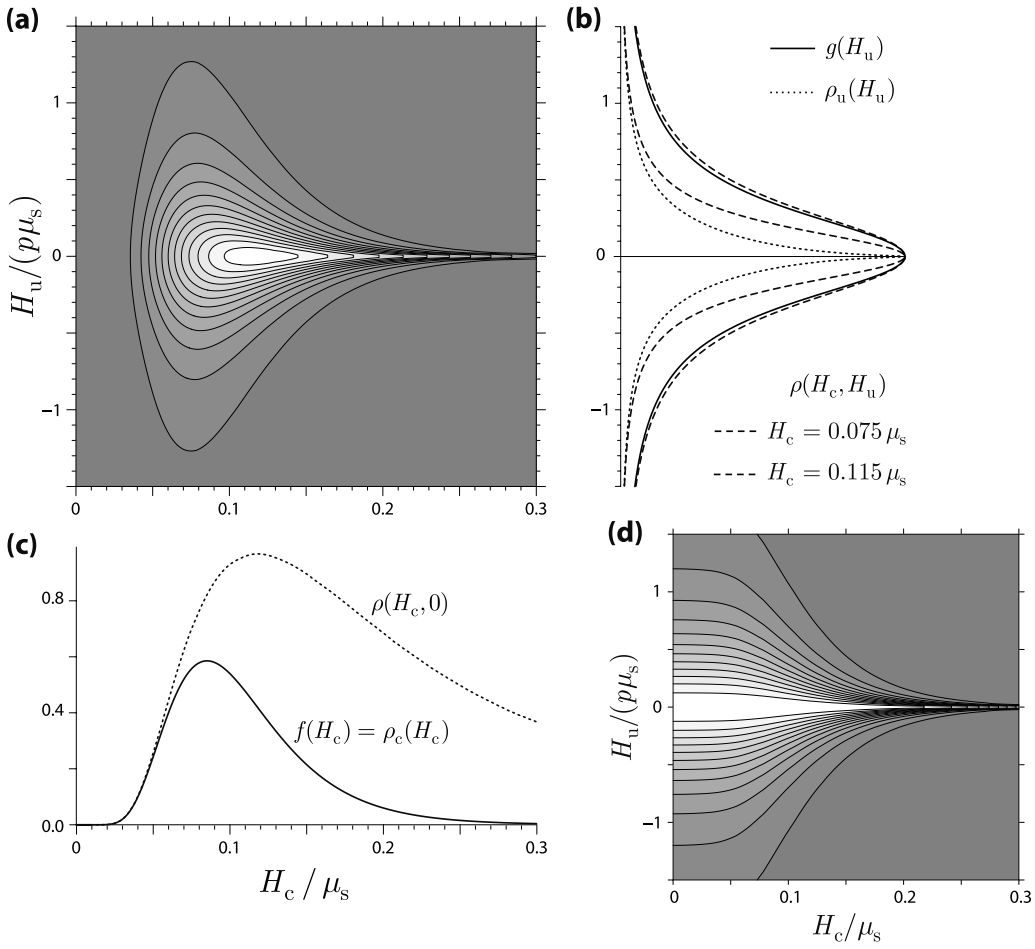

Figure 12. (a) The component P of the FORC function $\rho(H_c, H_u)$ of interacting S-W particles for the limit case of $p \rightarrow 0$. A logarithmic Gaussian distribution of microcoercivities with a median of $0.2\mu_s$ and a dispersion parameter of 0.4 has been assumed. The H_c and H_u axes are not to scale. (b) Profiles of $\rho(H_c, H_u)$ taken through the peak of ρ, at $H_c = 0.115\mu_s$, and through the maximum vertical spreading of the contour lines, at $H_c = 0.075\mu_s$ (dashed lines). The profiles are compared with the IFD (solid line) and the marginal distribution ρ_u. (c) Profile of $\rho(H_c, H_u)$ along the H_c axis (dotted line), and the marginal distribution ρ_c (solid line). (d) FORC function $\rho(H_c, H_u)$ normalized by $\rho(H_c, 0)$, whose contour lines reflect the dependence of w on H_c.

[36] The second term, Q, represents the combined effect of interactions and the reversible component of the elemental hysteresis loop. In the case of noninteracting S-W particles, Q coincides with the continuous part of the FORC function calculated by *Newell* [2005], whereby $Q(H_u > 0) \equiv 0$. As discussed by him, this contribution is sensitive to several phenomena such as thermal activations and noncoherent reversals of the magnetic moments. On the other hand, $Q \equiv 0$ for particles with perfect squared loops, since $\vartheta'(H) = 0$ within the integration limits of (32). Numerical calculations show that $Q(H_c, H_u > 0) \ll P$ for $\sigma_i \leq \sigma_K$, whereby $Q(H_u > 0) \rightarrow 0$ in the limit case of $p \rightarrow 0$ (Figure 11). The integral contribution of Q, however, does not depend on p and amounts to 45% in the case of S-W particles. This provides a simple explanation for the empirical observation that features related to the boomerang-shaped FORC function calculated by *Newell* [2005] are relatively weak in comparison to the peak along the H_c axis.

[37] An example of the component P of the FORC distribution calculated using (35) for the case of S-W particles with a logarithmic Gaussian distribution of coercivities is shown in Figure 12. The contours of the function have a clear tear-drop shape instead of the elliptical shape predicted by Preisach models. The shape of the contours is similar to that of FORC functions measured on highly dispersed SD particles (the "Kodak" samples in *Pike et al.* [1999]). Though the results of this section are based on the assumption of weak interactions, more concentrated SD samples, such as those measured by *Carvallo et al.* [2004] retain a hint of the same shape, especially in the upper half of the FORC space, together with the boomerang shape in the lower half predicted by *Newell* [2005].

[38] In the remaining part of this section I will discuss the relationship between the FORC function and the intrinsic properties of the sample, namely the coercivity distribution $f(H_c)$ and the IFD. Profiles of the FORC function along the H_c axis, denoted by $\rho(H_c, 0)$, and along H_u through the distribution peak, $\rho(H_c^{peak}, H_u)$, are commonly interpreted as rough estimates of the switching field and interaction field distributions, respectively [e.g., *Pike et al.*, 1999; *Carvallo*

et al., 2004]. The results shown in Figure 12 suggest a different interpretation. Equation (35) states that $\rho(H_c, 0)$ is proportional to $f(H_c)/w$, whereby it can be roughly assumed that $w(H_c) \approx F(H_c)$ (Figure 10). The resulting profile along the H_c axis is then proportional to $f(H_c)/F(H_c)$, which has a markedly different shape than $f(H_c)$, and no physical meaning. This result is the consequence of the fact that ρ is not a Preisach function. This might not be the case in strongly interacting samples, as demonstrated by the similarity of $\rho(H_c, 0)$ and $f(H_c)$ shown by *Carvallo et al.* [2004]. An intrinsically meaningful FORC parameter is the marginal distribution:

$$\rho_c(H_c) = \int_{-\infty}^{\infty} \rho(H_c, H_u) \mathrm{d}H_u \tag{36}$$

introduced by *Winklhofer and Zimanyi* [2006], which corresponds to the total magnetic contribution of all particles with switching field H_c. In case of weak interactions, it easy to show that $\rho_c \equiv f$ using (35) in (36).

[39] Profiles of the FORC function along H_u do not strictly coincide with the IFD, since w is also a function of H_u. However, in the case of weak interactions, $w(H_u)$ can be considered constant over the range if IF values, and $\rho(H_c, \zeta H_u)$ is proportional to the IFD produced by the proportion of all magnetic moment that remain constant when the sample is cycled from $-H_c$ to H_c. The total IFD is given by $\rho(0, \zeta H_u)$, since $w(H_c = 0) = 1$. Complications in using $\rho(0, \zeta H_u)$ to estimate the IFD in real measurements arise from a variety of features concentrated along the H_u axis, such as the "reversible ridge" introduced in the FORC data processing by *Pike* [2003] and viscosity effects observed by *Pike et al.* [2001]. However, $w(H_c)$ is close to unit for a range of H_c values left of the FORC peak, whereby H_u profiles of the FORC function taken in this region are similar to $\rho(0, H_u)$. The dependence of $\rho(H_c, H_u)$ is better visualized on a modified FORC diagram defined as

$$\rho^*(H_c, H_u) = \frac{\rho(H_c, H_u)}{\max\limits_{H_u} \rho(H_c, H_u)} \tag{37}$$

where the FORC function is normalized by its maximum value at a given H_c. In case of weak interactions, the maximum is centered at $H_u = 0$. The contours of ρ^* (H_c, H_u) have the same shape as $w(H_c)$, whereby the transition from $w \approx 1$ to $w \approx 0$ at intermediate values of H_c is evident. Unlike the case of $\rho(H_c, 0)$, the marginal distribution $\rho_u(H_u)$ obtained by integrating the FORC function over H_c is meaningless, as shown in Figure 12.

5. FORC Functions of Thermally Activated Particles

[40] Magnetic viscosity produces measurable effects on the shape of FORC diagrams, because of the finite time required to apply a magnetic field and perform a measurement. The effect is twofold: it produces a shift of the switching field distribution $f(H_c)$ toward lower fields, and it introduces an additional contribution to the FORC function along the negative H_u axis which is related to thermal relaxation effects that occurs at the inversion points $H_b = H_a$ [*Pike et al.*, 2001]. In the following, I will discuss a third effect that is phenomenologically equivalent to the presence of a virtual IF. This effect has consequences on the interpretation of FORC diagrams of weakly magnetic high-coercivity minerals, such as hematite and goethite.

[41] Thermal activations produce switching events that are not accounted by the FORC equation (30). Consider an isolated particle whose hysteresis loop is characterized by the two switching fields H_+ and H_-. Without thermal activations, $H_+ + H_- = 0$. The situation changes if the relaxation time of the particle is comparable with the measurement time: in this case $H_+ + H_- \neq 0$, whereby $H_+ + H_-$ is formally equivalent to an apparent IF H_q. This field is different for every particle and every switching event: therefore I assume H_q to be a statistical variable that is completely uncorrelated in space and time. *Néel* [1949] introduced H_q to account for the reduction of the switching field by thermal activations, and called it a "fluctuation field". In a single thermally activated particle, switching occurs at $H = \pm(H_{sw} - H_q)$, where H_q is a statistical variate with a PDF ξ_q. Thermal activation effects can be introduced in equation (30) by replacing the (thermally unactivated) switching fields $\pm H_{sw}$ with $\pm(H_{sw} - H_q)$. If q_a and q_b are two realizations of H_q at H_a and H_b, respectively, and $k(H_K, V)$ is the joint distribution of microcoercivities and volumes, equation (30) can be generalized to

$$\begin{aligned} M_\beta = & \iint_{H_K, V} k(H_K, V) \mathrm{d}H_K \mathrm{d}V \int_0^{\pi/2} \sin\varphi \mathrm{d}\varphi \\ & \cdot \iint_{x,y} \iint_{q_1, q_2} g_w(x) g_s(y) \xi_q(q_1) \xi_q(q_2) \\ & \cdot S_\beta \vartheta\left(S_\beta h_\beta / H_K\right) \mathrm{d}x \mathrm{d}y \mathrm{d}q_1 \mathrm{d}q_2 \end{aligned} \tag{38}$$

with integration limits:

$$\begin{aligned} \iint_{x,y} = & + \int_{x=-H_{sw}-H'_u+q_u}^{\infty} \int_{y=-H_{sw}-H'_b-x+q_b}^{H_{sw}+H'_a+x-q_a} (\uparrow\uparrow) \\ & + \int_{x=-\infty}^{-H'_u-q_c} \int_{y=H_{sw}-H'_b-x-q_b}^{\infty} + \int_{x=-H'_u-q_c}^{\infty} \int_{y=H_{sw}+H'_a+x-q_a}^{\infty} (\downarrow\uparrow) \\ & + \int_{x=-\infty}^{-H_{sw}-H'_u+q_u} \int_{y=-\infty}^{H_{sw}+H'_a+x-q_a} \\ & + \int_{x=-H_{sw}-H'_u+q_u}^{\infty} \int_{y=-\infty}^{-H_{sw}-H'_b-x+q_b} (\uparrow\downarrow) \\ & + \int_{x=-\infty}^{-H'_u-q_c} \int_{y=H_{sw}+H'_a+x-q_a}^{H_{sw}-H'_b-x-q_b} (\downarrow\downarrow) \end{aligned} \tag{39}$$

whereby $q_u = (q_b + q_a)/2$, and $q_c = (q_b - q_a)/2$.

[42] The PDF of H_q can be calculated from the solution of the kinetic equation of a uniaxial SD grain in the framework of Néel's theory. I thereby assume that the probability P of a moment switching occurring in a field $H = \pm(H_{sw} - H_q)$ in a single particle is proportional to the magnetization acquired by a large number of particles in a initial demagnetization state under the same conditions. Using the relaxation time estimate of *Néel* [1949], the probability of a moment switching in a field $H = \pm(H_{sw} - H_q)$ within a given time interval t is given by

$$P(H_q) = \exp\left[-f_0 t e^{-E_0\left(H_q/H_K\right)^2}\right] \tag{40}$$

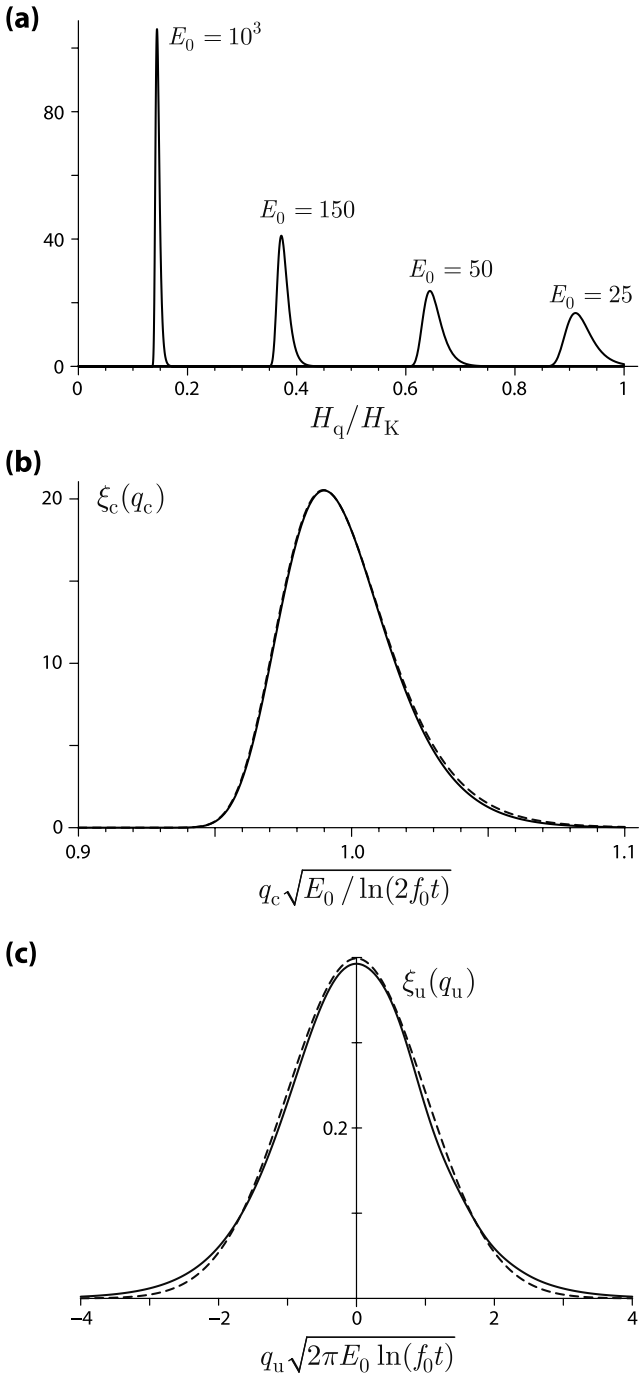

Figure 13. (a) The PDF of the thermal fluctuation field H_q for various amplitudes of the normalized energy barrier E_0 that span form typical values for stable SD grains (E_0 = 1000), to SD grains at the SD/superparamagnetic threshold (E_0 = 25). (b) The PDF of h_c (solid line), and the approximation given by equation (42) (dashed line). (c) The PDF of h_u (solid line), and the approximation given by equation (42) (dashed line).

where E_0 is the energy barrier of a particle normalized by the thermal energy k_BT, and $f_0 \approx 10$ GHz is the atomic reorganization frequency. In the noninteracting case, $E_0 = \mu_0 V M_s H_K/(2k_BT)$, whereby this result holds also for weakly interacting systems if $\sigma_i \ll H_K$. In strongly interacting systems, the contribution of the IF to the energy barrier must be considered as well. The derivative of (40) with respect to H_q gives the PDF of $h_q = H_q/H_K$:

$$\xi_q(h_q) = 2f_0tE_0h_qe^{-E_0h_q^2}\exp\left[-f_0te^{-E_0h_q^2}\right] \tag{41}$$

(Figure 13a). Since q_c and q_u are the sum and the difference of the independent variates q_b and q_a, respectively, the corresponding PDFs are given by $\xi_c(2q_c) = \xi_q(q_u) * \xi_q(q_u)$ and $\xi_u(2q_u) = \xi_q(q_u) * \xi_q(-q_u)$. Analytical solutions for ξ_c and ξ_u cannot be found, however, good approximations are provided by:

$$\xi_c(x) \approx 2\pi^{(\pi-1)/2}(f_0t)^{\pi/2}E_0xe^{-\pi E_0x^2/2}\exp\left[-2f_0te^{-E_0x^2}\right]$$
$$\xi_u(x) \approx \varepsilon e^{-\pi(\varepsilon x)^2} \tag{42}$$

with $\varepsilon = \sqrt{E_0\ln(f_0t)}$. $\xi(q_c)$ is a positive PDF with expected value $\bar{h}_q = \sqrt{\ln(2f_0t)/E_0}$ that coincides with Néel's definition of fluctuation field. On the other hand, $\xi(q_u)$ is a Gaussian function with zero mean and standard deviation $\sigma_q = [2\pi E_0 \ln(f_0t)]^{-1/2}$ (Figure 13).

[43] Again, I limit the calculation of the FORC function to the case of weak interactions, defined in section 4.4. Using the same assumptions and simplifications, the term P of the FORC function is given by

$$P = \frac{1}{ws}\iint_{H_K,V} k(H_K,V)\mathrm{d}H_K\mathrm{d}V\int_0^{\pi/2}\bar{\vartheta}(h_{sw})\sin\varphi\mathrm{d}\varphi \cdot\int_0^{\infty}\xi_c(q_c)g_s\left(\frac{H_K(h_{sw}-q_c)-H_c'}{s}\right)\mathrm{d}q_c \cdot\int_{-\infty}^{\infty}\xi_u(q_u)g_w\left(\frac{H_u'-H_Kq_u}{w}\right)\mathrm{d}q_u \tag{43}$$

Since the reversible part of the elemental hysteresis loops is modified by thermal activations, $\vartheta(H)$ is no longer given by the S-W theory. Since $\vartheta(H)$ has the same effect as a multiplicative factor, I will discard the angular dependence integral in (43), assuming $h_{sw} \approx 0.5$. If $k(H_K, V)$ is a broad distribution, g_s can be considered equivalent to a Dirac δ function, and (43) simplifies to

$$P \propto \frac{1}{w}\iint_{H_K,V} k(H_K,V)\xi_c(1/2-H_c/H_K)\mathrm{d}H_K\mathrm{d}V \cdot\int_{-\infty}^{\infty}\xi_u(q_u)g_w\left(\frac{H_u'-H_Kq_u}{w}\right)\mathrm{d}q_u \tag{44}$$

The noninteracting case is given by

$$P \propto \frac{1}{w}\iint_{H_K,V} k(H_K,V)\xi_c(1/2-H_c/H_K)\xi_u(H_u/H_K)\mathrm{d}H_K\mathrm{d}V \tag{45}$$

which has a finite width along H_u. The half width of $P(H_c^{peak}, H_u)$ is controlled by ξ_u, and it is roughly given by $4H_c^{peak}[2\pi E_0\ln(f_0t)]^{-1/2}$. The noninteracting case is of particular interest when FORCs of low-μ_s minerals are measured. For example, μ_s of hematite and goethite is $\leq$2.5 kA/m. Assuming a maximum random packing fraction of 0.7 and using (17) the maximum possible half width of the IFD is $0.13\mu_s$, which corresponds to barely 0.4 mT for pure

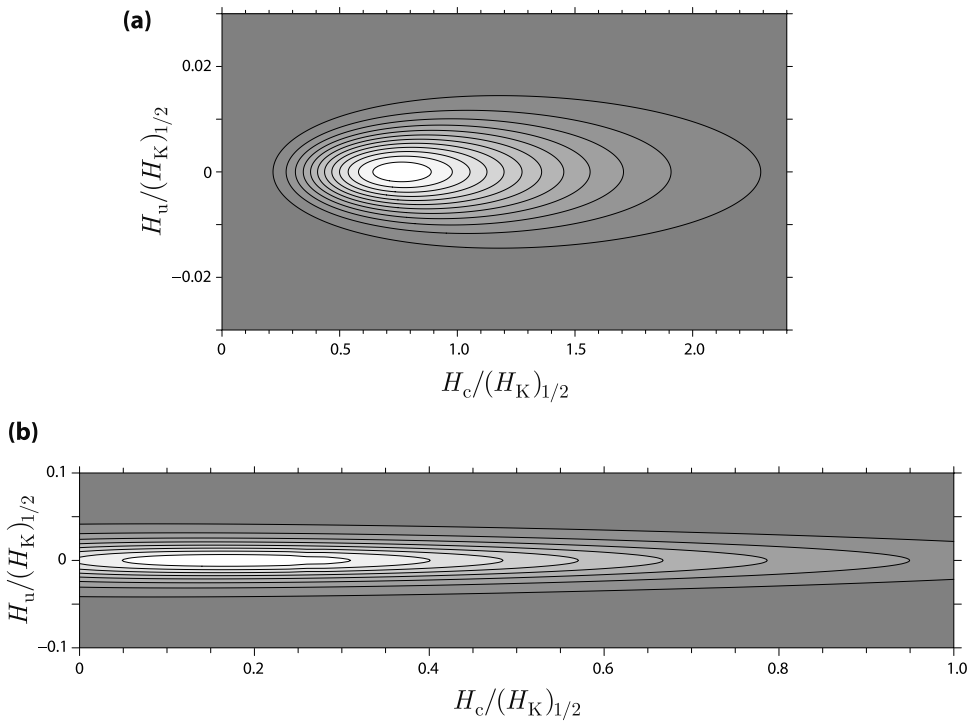

Figure 14. Two examples of FORC functions of noninteracting, thermally activated SD grains with a joint microcoercivity and volume distribution $k(H_K, V) = \kappa(H_K)v(V)$, where $\kappa(H_K)$ is a logarithmic Gaussian distribution with median $(H_K)_{1/2}$ and dispersion parameter equal to 0.4. (a) Volume distribution is a logarithmic Gaussian function with dispersion parameter equal to 0.5 and the median chosen so, that $E_0 = 1000$ when $H_K = (H_K)_{1/2}$. The parameters are typical of stable SD grains. Notice that the H_u scale has been exaggerated by a factor 20. (b) Volume distribution is a logarithmic Gaussian function with dispersion parameter equal to 0.5 and the median chosen so, that $E_0 = 100$ when $H_K = (H_K)_{1/2}$. The H_c and H_u axes are on scale.

hematite or goethite samples. The FORC function of such minerals is therefore not expected to show any visible vertical spreading for $H_c > 0$, except for smoothing effects related to data processing. FORC diagrams of these minerals, however, do have a distribution along H_u that cannot be explained by dipole interactions, nor by processing artifacts. For example, the FORC diagram of synthetic hematite of *Pike et al.* [2001] is characterized by a vertical half width of ≈10 mT. This feature can be well explained using (45).

[44] Examples of FORC functions calculated for thermally activated, noninteracting particles are shown in Figure 14. The distributions ξ_c and ξ_u are weak functions of t, which in turn depends in a complex manner on H_a and H_b. Because of the weak dependence of ξ_c and ξ_u on t, a rough model for the timing of FORC measurements is sufficient. Each step requires a constant measurement time t_m. If the field H is ramped at a constant rate, the effective duration of H can be assumed to be $r|H|$, where r is a constant that depends on the ramp rate. Since H_u is small compared to H_c in the models shown in Figure 14, the total time during which the field is applied is given by $t \approx t_m + rH_c$. Distributions of microcoercivities and volumes can be modeled using logarithmic Gaussian functions with appropriate parameters, however, the joint distribution $k(H_K, V)$ requires some knowledge about the correlation between H_K and V. The simplest model, $k(H_K, V) = \kappa(H_K)v(V)$, assumes that H_K and V are independent. Experimental reconstructions of $k(H_K, V)$ on samples containing superparamagnetic particles show a very weak inverse correlation such that $H_K \propto V^{-1/3}$ [*Jackson et al.*, 2006]. Therefore I will use the simple model $k(H_K, V) = \kappa(H_K)v(V)$ in equation (45).

[45] The synthetic examples of Figure 14 show that the peak of the FORC functions moves toward $H_c = 0$ when the energy barrier is progressively decreased, whereby initially closed contour lines start to intersect the H_u axis. At this point some particles are effectively superparamagnetic and exit the FORC space. The corresponding FORC function is similar to the FORC diagram of synthetic hematite measured by *Pike et al.* [2001].

6. Using FORC Distributions to Estimate the IFD

[46] In section 4, a clear relationship between H_u profiles of the FORC function and the IFD was established for the case of small interactions. The upper half of the FORC diagram is almost not affected by the reversible component of the elemental hysteresis loops, and this is the part of the diagram that is more closely related to dipole interactions. Is then a quantitative interpretation of the FORC diagram possible? In principle, $H_u > 0$ profiles are functions of the form given in equation (17), which can be used to fit the measured data. However, this approach is complicated by the fact that the profiles may depend strongly on H_c (Figure 12).

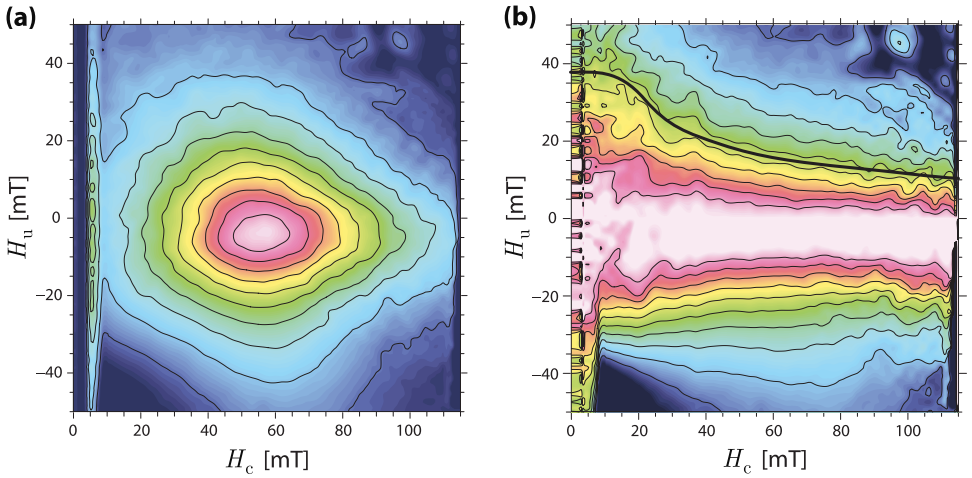

Figure 15. (a) FORC diagram of an organic rest found in a sediment from lake Baikal (Russia). (b) FORC function has been normalized according to equation (37). The contours show the same trend (marked by the thick black line) as in Figure 12d; however, the dependence of the normalized FORC function on H_c is much less pronounced.

[47] Another complication concerns specifically the interpretation of FORCs measured on natural samples, because these samples are not necessarily homogeneous, since they may contain different magnetic components. This means that not every particle is interacting with every other in the statistical sense given by full randomness. Furthermore, it is reasonable to assume that magnetic components with different origins are associated to grains that are located in different regions of the sample. For example, authigenic minerals in a sediment might be concentrated in "spots" that were rich in organic matter. It is therefore possible that strong interactions exist within the grains of one component, but not between the grains of different components. In such cases, the H_c dependence of H_u profiles can differ strongly from that of a homogeneous sample. If particle groups having different coercivities are geometrically "isolated", H_u and H_c become uncorrelated, and the FORC function apparently coincides with the basic Preisach model described in section 4.1. FORC functions of natural samples are probably intermediate between (a) the strong $H_u - H_c$ correlation of Figure 12, which represents the case of one homogeneously dispersed component, and (b) a "Preisach-like" case created by a number of well-separated particle clusters with different coercivities. An example of such situation is provided by the lake sediment of Figure 15, which was described by *Egli* [2004]. The sample is a small organic rest containing a high concentration of magnetosomes. As show by the normalized FORC function, H_u profiles tend to narrow toward higher H_c values, however, the H_c dependence of these profiles is very weak in comparison to Figure 12. This result can be eventually explained by magnetosomes and magnetosome chains concentrated in "spots" that provided the appropriated living conditions for the bacteria on a microscopic scale.

[48] Synthetic samples should provide a closer analogy to the model of section 4, as demonstrated by the case of highly dispersed SD particles shown by *Pike et al.* [1999]. Is this analogy also valid at higher particle concentrations? To investigate this possibility, I used equations (30)–(32) to model the FORC diagram of acicular SD maghemite measured at room temperature by *Carvallo et al.* [2004]. The particles are randomly oriented and they are not expected to reverse by coherent rotation. Therefore both the S-W and the rectangular loop model discussed in section 4 are not appropriate. However, the FORC function has a negative region, as predicted by *Newell* [2005]: therefore I chose the S-W model as the closest analogon to the maghemite particles. As discussed in section 4, the reversible component of the elemental loops has only a minor influence on the central peak of the FORC function. Equations (30)–(32) must be solved iteratively, using some arbitrary starting parameters. The saturation magnetization of the particles is 322 kA/m [*Carvallo et al.*, 2004]. I assumed a microcoercivity distribution $\kappa(H_K) = M'_{IRM}(0.5H_K)$, where M'_{IRM} is the derivative of the IRM acquisition curve reported by *Carvallo et al.* [2004]. Initial values of w and s were calculated for the noninteracting case. The H_u profile through the peak was fitted using equation (17) to obtain the initial estimate $p = 0.077$ of the packing fraction. The dependence of the IFD on the magnetization was not considered in this model, since the IFD is not very sensitive to the alignment of the particles if $p < 0.1$. Each iteration gives new estimates of w, s. A new estimate of p was obtained using $p_{i+1} = p_i/a$, where a is the factor needed to obtain the closest match between the measurement $\rho_m(H_c^{peak}, H_u)$ and the scaled model $\rho(H_c^{peak}, aH_u)$. After three iterations, the model converged to a stable solution with $p = 0.10$ that closely matched the measurement (Figure 16). The overall shape of the FORC profile, as well as the slight asymmetry between the $H_u > 0$ and $H_u < 0$ regions, are correctly reproduced. Since the computation of (31)–(33) is extremely slow, it was not possible to extend the calculations to the entire FORC space. This fit demonstrates that a quantitative interpretation of the FORC diagram is possible, however, the abovementioned approach is unpractical for routine applications.

7. Conclusions

[49] A strictly quantitative theory of dipolar interactions and their appearance in FORCs of thermally activated SD

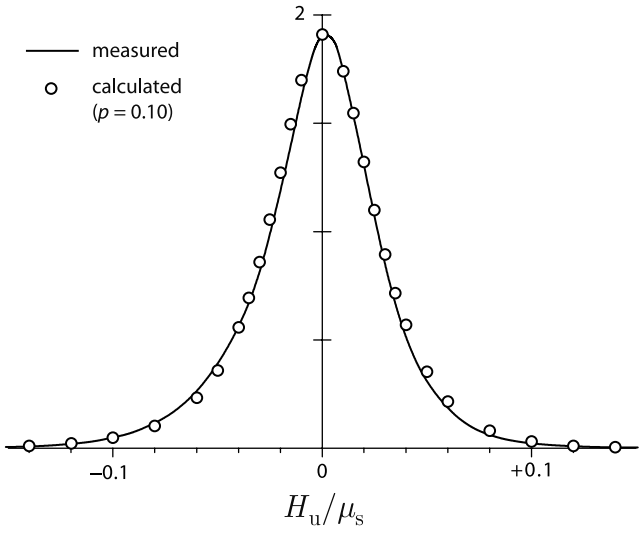

Figure 16. A best fit of the FORC model given by equations (30)–(32) to the FORC diagram of acicular maghemite measured at room temperature by *Carvallo et al.* [2004]. A profile of the FORC function through the peak is shown. The model fits accurately the measured data, including the slight asymmetry between the regions defined by $H_u > 0$ and $H_u < 0$. The packing fraction resulting after 3 iterations is $p \approx 0.1$.

particles has been developed. Although the general equations developed can be evaluated analytically only in the limit case of weak interactions, the special cases discussed in this paper provide a deeper understanding of FORC diagrams. I summarize the main conclusions in following points:

[50] 1. The IFD is effectively independent of the magnetization state for packing fractions $p < 0.1$. Above this limit, the IFD of particles with aligned moments diverges from that of other configurations. The IFD of partially aligned dipoles is obtained by considering the weighted superposition of the IFDs produced by random and aligned dipoles. It was shown that the IFD produced by any magnetization configuration corresponds either to the case of random dipoles, or to that of partially aligned dipoles.

[51] 2. The complexity of FORC models is greatly reduced if the three-dimensional IF is replaced by a scalar IF. The scalar IF is equal to the IF component along the measurement direction, multiplied by a factor ζ that depends on the reversing mode of the particles. The three special cases of particles with squared hysteresis loops, S-W particles, and particles that reverse by curling are characterized by $\zeta = 1$, $\zeta = 1.354$ and $\zeta \approx 1.58$, respectively.

[52] 3. The IF is not constant during a FORC measurement, whereby the fundamental assumptions of the basic Preisach model is violated. The IF is correctly modeled as sum of three contributions. The first contribution is the field produced by the component w of the magnetic moments that did not change when the sample was cycled from H_a to H_b. The second contribution is the IF produced by the component s of the magnetic moments that switched upon cycling from H_a to H_b. The third contribution is a virtual IF that arises from thermal activations. The first two contributions are controlled by the same realization of the statistical variates H_w and H_s, whereas the third contribution is represented by two independent realizations of a statistical variate H_q in H_a and H_b.

[53] 4. A general estimate of the FORC function is provided by the iterative evaluation of equations (30)–(32) and (38)–(39), starting from arbitrary initial conditions, such as those described in section 6. The equations involve four-dimensional integrals of numerical solutions for the equilibrium position of a magnetic moment in an applied field. Their evaluation is therefore very time consuming.

[54] 5. A simple approximated solution can be obtained for weak interactions. In this case, the FORC function is the sum of two contributions, P and Q. P is a symmetric function about the H_c axis, and represents the intrinsic contribution of dipolar interactions. This contribution produces tear-drop-shaped contour lines in the FORC space, which clearly indicate that P is not a Preisach function. Q represents the contribution of the reversible component. In the noninteracting case, Q corresponds to the continuous component of the FORC function calculated by *Newell* [2005]. This component depends on the switching mode of the particles and is influenced by thermal activations. It contributes mainly to the lower half of the FORC space, defined by $H_u < 0$, and is negligible if $H_u > 0$. The total contributions of P and Q to the FORC function are obtained by integration over the FORC space. The total relative contribution of P is 1 in the case of squared elemental hysteresis loops, and 0.542 for S-W particles.

[55] 6. A physical interpretation of the FORC function $\rho(H_c, H_u)$ of weakly interacting, nonthermally activated particles is best provided by the positive half of H_u profiles $\rho\,(H_c \rightarrow 0, H_u > 0)$, and by the marginal distribution $\rho_c(H_c)$ defined in equation (36). The marginal distribution coincides with the effective coercivity distribution of the particles, and $\rho(H_c \rightarrow 0, H_u)$ coincides with the scaled IF distribution $W(H, p, \zeta\mu_s)$. Since secondary features related to thermal activation effects and data processing may appear along the H_u axis, profiles taken left from the peak of the FORC function provide a good estimate of the IDF.

[56] 7. The FORC function of noninteracting, thermally activated particles has a finite vertical spreading that should not be confused with the effect of dipolar interactions. It is observed in FORCs of weakly magnetic minerals, such as hematite and goethite, where dipolar interactions are negligible.

[57] **Acknowledgments.** This work was supported by grant 0309291 from the Geophysics Program of the Earth Science Division of the National Science Foundation. This is IRM publication 0608. I am deeply grateful to Andrew Newell and an anonymous reviewer for their interesting comments that improved the original manuscript significantly. I also would like to thank Claire Carvallo for kindly providing the data for the acicular maghemite sample.

References

Aharoni, A. (1999), Curling reversal mode in nonellipsoidal ferromagnetic particles, *J. Appl. Phys.*, *86*, 1041–1046.

Anderson, P. W. (1950), Pressure broadening of the ammonia inversion line by foreign gases: Quadrupole-induced dipole interaction, *Phys. Rev.*, *80*, 511–513.

Berkov, D. V. (1996), Local-field distribution in systems with dipolar interparticle interactions, *Phys. Rev. B*, *53*, 731–734.

Bracewell, R. (1986), *The Fourier Transform and Its Applications*, 2nd ed., McGraw-Hill, New York.

Carvallo, C., Ö. Özdemir, and D. J. Dunlop (2004), First-order reversal curve (FORC) diagrams of elongated single-domain grains at high and low temperatures, *J. Geophys. Res.*, *109*, B04105, doi:10.1029/2003JB002539.

Carvallo, C., D. Dunlop, and Ö. Özdemir (2005), Experimental comparison of FORC and remanent Preisach diagrams, *Geophys. J. Int.*, *162*, 747–754.

Cerchez, M., L. Stoleriu, and A. Stancu (2004), Interaction effects in high density magnetic particulate media, *Physica B*, *343*, 48–52.

Della Torre, E. (1965), Effect of interaction on the magnetization of single domain particles, *IEEE Trans. Audio Electroacoust.*, *14*, 86–93.

Dormann, J. L., D. Fiorani, and E. Tronc (1997), Magnetic relaxation in fine-particle systems, *Adv. Chem. Phys.*, *98*, 283–494.

Dunlop, D. J., M. Wescott-Lewis, and M. Bailey (1990), Preisach diagrams and anhysteresis: do they measure interactions?, *Phys. Earth. Planet. Inter.*, *65*, 62–67.

Egli, R. (2004), Characterization of individual rock magnetic components by analysis of remanence curves, 1. Unmixing natural sediments, *Stud. Geophys. Geod.*, *48*, 391–446.

Egli, R. (2006), Theoretical considerations on the anhysteretic magnetization of interacting particles with uniaxial anisotropy, *J. Geophys. Res.*, *111*, B12S18, doi:10.1029/2006JB004577.

Hejda, P., and T. Zelinka (1990), Modeling of hysteresis processes in magnetic rock samples using the Preisach diagram, *Phys. Earth Planet. Inter.*, *63*, 32–40.

Jackson, M., B. Carter-Stiglitz, R. Egli, and P. Solheid (2006), Characterizing the superparamagnetic grain distribution $f(V, H_k)$ by thermal fluctuation tomography, *J. Geophys. Res.*, doi:10.1029/2006JB004514, in press.

Man, W., A. Donev, F. Stillinger, M. Sullivan, W. Russel, D. Heeger, S. Inati, S. Torquato, and P. Chaikin (2005), Experiments on random packing of ellipsoids, *Phys. Rev. Lett.*, *94*, 198001.

Mayergoyz, I. D. (1986), Mathematical models of hysteresis, *IEEE Trans. Magn.*, *MAG-22*, 603–608.

Mayergoyz, I. D. (1991), *Mathematical Models of Hysteresis*, Springer, New York.

Muxworthy, A., and W. Williams (2005), Magnetostatic interaction fields in first-order-reversal curve diagrams, *J. Appl. Phys.*, *97*, 063905.

Muxworthy, A., D. Heslop, and W. Williams (2004), Influence of magnetostatic interactions on first-order-reversal curve (FORC) diagrams: a micromagnetic approach, *Geophys. J. Int.*, *158*, 888–897.

Néel, L. (1949), Théorie du trainage magnétique des ferromagnétiques en grains fins avec applications aux terres cuites, *Ann. Geophys.*, *5*, 99–136.

Néel, L. (1954), Remarques sur la théorie des propriétés magnétiques des substances dures, *Appl. Sci. Res., Sect. B*, *4*, 13–24.

Newell, A. J. (2005), A high-precision model of first-order reversal curve (FORC) functions for single-domain ferromagnets with uniaxial anisotropy, *Geochem. Geophys. Geosyst.*, *6*, Q05010, doi:10.1029/2004GC000877.

Onoda, G. Y., and E. G. Liniger (1990), Random loose packing of uniform spheres and the dilatancy onset, *Phys. Rev. Lett.*, *64*, 2727–2729.

Pardavi-Horvath, M., E. Della Torre, and F. Vajda (1993), A variable variance Preisach model, *IEEE Trans. Mag.*, *29*, 3793–3795.

Pike, C. R. (2003), First-order reversal-curve diagrams and reversible magnetization, *Phys. Rev. B*, *68*, 104424.

Pike, C. R., A. P. Roberts, and K. L. Verosub (1999), Characterizing interactions in fine magnetic particle systems using first order reversal curves, *J. Appl. Phys.*, *85*, 6660–6667.

Pike, C. R., A. P. Roberts, and K. L. Verosub (2001), First-order reversal curve diagrams and thermal relaxation effects in magnetic particles, *Geophys. J. Int.*, *145*, 721–730.

Pike, C. R., C. A. Ross, R. T. Scalettar, and G. Zimanyi (2005), First-order reversal curve diagram analysis of a perpendicular nickel nanopillar array, *Phys. Rev. B*, *71*, 134407.

Preisach, F. (1935), Über die magnetische Nachwirkung, *Z. Phys.*, *94*, 277–302.

Roberts, A. P., C. R. Pike, and K. L. Verosub (2000), First-order reversal curve diagrams: A new tool for characterizing the magnetic properties of natural samples, *J. Geophys. Res.*, *105*, 28,461–28,475.

Shcherbakov, V. P., and V. Shcherbakova (1975), On the magnetostatic interaction in a system of single-domain grains, *Izv. Earth Phys.*, *9*, 101–104.

Shcherbakov, V. P., and N. K. Sycheva (1996), Monte Carlo modeling of TRM and CRM acquisition and comparison of their properties in an ensemble of interacting SD grains, *Geophys. Res. Lett.*, *23*, 2827–2830.

Sornette, D. (2004), *Critical Phenomena in Natural Sciences*, 2nd ed., 523 pp., Springer, New York.

Stancu, A., L. Stoleriu, and M. Cerchez (2001), Micromagnetic evaluation of magnetostatic interactions distribution in structured particulate media, *J. Appl. Phys.*, *89*, 7260–7262.

Stoner, E. C., and E. P. Wohlfarth (1948), A mechanism for hysteresis in heterogeneous alloys, *Philos. Trans. R. Soc. London, Ser. A*, *240*, 599–642.

Sugiura, N. (1979), ARM, TRM, and magnetic interactions: concentration dependence, *Earth Planet. Sci. Lett.*, *42*, 451–455.

Talbot, J., P. Schaaf, and G. Tarjus (1991), Random sequential addition of hard spheres, *Molec. Phys.*, *72*, 1397–1406.

Winklhofer, M., and G. T. Zimanyi (2006), Extracting the intrinsic switching field distribution in perpendicular media: a comparative analysis, *J. Appl. Phys.*, *99*, 08E710.

R. Egli, Institute for Rock Magnetism, University of Minnesota, Minneapolis, MN 55455, USA. (e.g.lix007@umn.edu)